Electronic defects in Cu(In, Ga)Se₂: Towards a comprehensive model

Conrad Spindler, Finn Babbe,[*] Max Hilaire Wolter, Florian Ehré, Korra Santhosh,[†] Pit Hilgert,
Florian Werner, and Susanne Siebentritt[‡]

*Laboratory for Photovoltaics, Physics and Materials Science Research Unit, University of Luxembourg,
44, rue du Brill, 4422 Belvaux, Luxembourg*

The electronic defects in any semiconductor play a decisive role for the usability of this material in an optoelectronic device. Electronic defects determine the doping level as well as the recombination centers of a solar cell absorber. Cu(In, Ga)Se₂ is used in thin-film solar cells with high and stable efficiencies. The electronic defects in this class of materials have been studied experimentally by photoluminescence, admittance, and photocurrent spectroscopies for many decades now. The literature results are summarized and compared to new results by photoluminescence of deep defects. These observations are related to other experimental methods that investigate the physicochemical structure of defects. To finally assign the electronic defect signatures to actual physicochemical defects, a comparison with theoretical predictions is necessary. In recent years the accuracy of these calculations has greatly improved by the use of hybrid functionals. A comprehensive model of the electronic defects in Cu(In, Ga)Se₂ is proposed based on experiments and theory. The consequences for solar cell efficiency are discussed.

I. INTRODUCTION

Solar cells based on the chalcopyrite Cu(In,Ga)Se₂ have seen dramatic efficiency improvements in the last years, reaching 20.4% for flexible solar cells [1] and 23.3% for rigid solar cells [2–4]. These record cells are based on the alloy of CuInSe₂ and CuGaSe₂ with about 30% of the Ga compound. Additionally, the ternary end compositions are interesting as bottom [5,6] and top cells [7] in thin-film tandem applications [8]. For further improvement of these solar cells, a detailed knowledge of the electronic structure will be indispensable. Electronic states in the band gap caused by defects, acting as shallow donors and acceptors, are responsible for the doping level and thus the band bending, as well as for the radiative recombination in the solar cell. On the other hand, deep states contribute to nonradiative recombination. In Cu(InGa)Se₂, these defect states are generally due to native defects. Although the absorbers in the solar cells are doped by various alkalis, these impurities do not form states in the band gap [9]. For an understanding of defects in the alloy Cu(In, Ga)Se₂ it is necessary to study the ternary end compositions CuInSe₂ and CuGaSe₂ to avoid the effects of alloy disorder. After decades of experimental and theoretical research, a comprehensive model of the electronic defects is now emerging.

We review new and previously published experimental evidence for electronic defects and compare it to information on structural defects, as well as to recent calculations, based on hybrid functionals. We make use of the fundamental differences in the electronic structure between stoichiometric material grown under copper excess, labeled Cu-rich, and material grown under copper deficiency, labeled Cu-poor, which were first pointed out by Zott *et al.* [10] and explained by Dirnstorfer *et al.* [11]. The pseudobinary phase diagram between In₂Se₃ or Ga₂Se₃ and Cu₂Se [12–14] already illustrates the difference: single-phase chalcopyrite exists on the Cu-poor side with several percent Cu deficiency, whereas on the Cu-rich side a two-phase system exists with stoichiometric chalcopyrite and Cu₂Se, which takes up the Cu excess. The broad existence region on the Cu-poor range is possible only by the formation of defects such as Cu vacancies V_{Cu} or element III on copper antisites In_{Cu} or Ga_{Cu}. While the Cu-poor material is compensated [11], i.e., it contains high concentrations of both acceptors and donors, the chalcopyrite grown under Cu excess is stoichiometric with much lower defect densities [15]. Interestingly, high-efficiency solar cells are made from Cu-poor material [15].

Information on the energies of electronic defects can be obtained by photoluminescence spectroscopy (PL) and by the analysis of the temperature dependence of Hall or capacitance measurements, such as deep-level transient spectroscopy (DLTS) or admittance spectroscopy (AS), as well as transient transport measurements such as modulated photocurrent (MPC) or photoinduced current transients (PICT). In the following, we concentrate first on bulk methods such as PL and Hall measurements and compare them later to the results of other measurements. We concentrate on measurements that result in definite defect energies and compare these energies to the results obtained from a range of recent calculations based
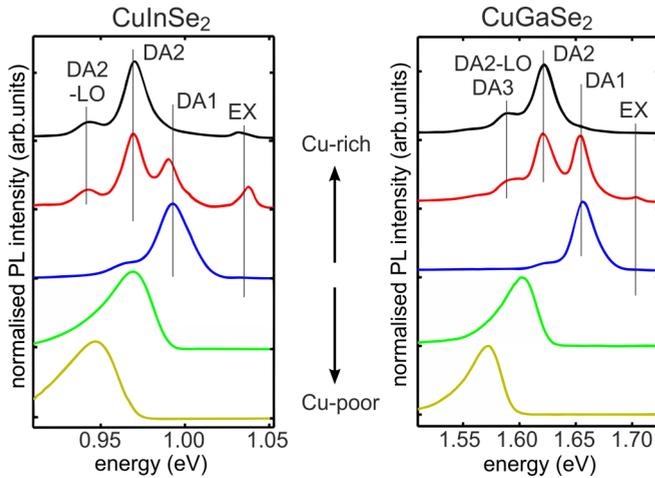
FIG. 1. Spectra of the near-band-edge luminescence of epitaxial $CuInSe_2$ and $CuGaSe_2$ films on GaAs with varying Cu content, measured at 10 K. The blue spectra in both cases are measured on approximately stoichiometric material, red and black on Cu-rich, green and olive on Cu-poor films. DA stands for donor-acceptor pair transition, DA-LO for the phonon replica of a DA transition, and EX for an excitonic transition. The spectra of Cu-poor chalcopyrites are redshifted and broadened by potential fluctuations, whereas the Cu-rich material shows narrow lines, which allow the detection of shallow defects. The similarity between the sets of spectra is remarkable and indicates that the shallow defects are very similar in $CuInSe_2$ and $CuGaSe_2$. Adapted from [15].

on hybrid functionals to derive a comprehensive defect model. Finally, we discuss the consequences for solar cells.

II. SHALLOW DONORS AND ACCEPTORS

A. Two acceptors and a donor

Information on shallow donors and acceptors comes from near-band-edge PL spectra and their intensity and temperature dependence. An overview of the low-temperature PL spectra of $CuInSe_2$ and $CuGaSe_2$ with varying Cu content is given in Fig. 1 [15]. The figure shows the spectra obtained from epitaxial films grown by MOVPE (metallorganic vapor phase epitaxy) on GaAs. The compositional dependence of the near-band-edge luminescence of polycrystalline films on Mo-covered glass shows exactly the same trends [11,16–18].

Both Cu-poor $CuInSe_2$ and $CuGaSe_2$ show broad asymmetric luminescence which increasingly shifts to lower energies with decreasing Cu content. This behavior is explained by fluctuating electrostatic potentials [11,19–21]. In a compensated p-type semiconductor with high densities of donors and acceptors, most of the acceptors and all of the donors are charged, even at very low temperatures. In fact, an increasing density of donor- and acceptor-type defects has been observed by neutron scattering with increasing Cu deficiency [22] (see Sec. IV B below). The majority of these defects can be expected to be combined into neutral defect complexes [22–24]. The density of remaining single defects is still high enough to cause electrostatic potential fluctuations, since their spatial distribution always shows some statistical fluctuations, causing spatially separated areas with different charges. These

net charged areas in turn cause spatial fluctuations of the electrostatic potential, particularly at low temperatures, since then they are not screened by free carriers [25,26]. Although some dielectric screening of these charges is possible, the Debye screening length at low temperatures will be very long, on the order of several 100 nm. With increasing copper deficit the degree of compensation increases and shifts the PL peak to lower energies. In the Cu-poor range of compositions, the peak positions of the photoluminescence spectra are thus determined by the degree of compensation [27] and are not suitable for defect spectroscopy.

Cu-rich material, on the other hand, shows narrow peaks. By detailed excitation and temperature-dependent studies [19,20,28], the different peaks can be assigned to donor-acceptor pair transitions (DA) and to excitonic transitions (EX), as indicated in Fig. 1. We observe three transitions that show DA character; the two high-energy ones are labeled DA1 and DA2 and are discussed in this section. The highest energy transition is an excitonic transition. This assignment is in agreement with a wide range of earlier and later results from the literature. The first PL studies on $CuInSe_2$ were performed on single crystals, and still the luminescence lines were rather broad [29–31]. Among the first to observe narrow donor-acceptor transitions was Abou-Elfotouh *et al.* [32], albeit they interpret the DA transitions falsely as excitons. The early work of Niki *et al.* [33–35] was based on high-quality thin films and crystals and allowed pioneering investigation of the temperature and intensity dependencies of the observed PL spectra. Since then more agreement has been reached for the attribution of the various PL peaks to specific electronic transitions: for the excitons in $CuInSe_2$ see, e.g., [20,35–40]; for those in $CuGaSe_2$ see, e.g., [19,38,41–46]; for the DA or the related free-to-bound (FB) transitions in $CuInSe_2$ see, e.g., [18,20,33,37,47]; and in $CuGaSe_2$ see, e.g., [19,42,47–49]. When investigating the temperature dependence of the luminescence spectra we observe the change from DA luminescence to FB luminescence. The defect that becomes ionized first with increasing temperature is the shallower one. It is most likely that this is a donor and not an acceptor, because the effective mass of electrons is smaller than that of holes in most direct semiconductors, so in $CuInSe_2$ [50–54] and in $CuGaSe_2$ [46,54], which leads to shallower donor states than acceptor states, as predicted by the hydrogen model (see, e.g., [55]). The transition from DA luminescence to FB luminescence is more clearly seen in $CuGaSe_2$ [19] than in $CuInSe_2$ [20]. The larger difference between DA and FB in $CuGaSe_2$ is expected for a hydrogenlike donor, since the donor would be somewhat deeper in $CuGaSe_2$ than in $CuInSe_2$ because of the higher effective electron mass and lower dielectric constant in $CuGaSe_2$. (For an overview of material parameters see [28] or [56]; for a prediction on effective masses see [54]. From these values the hydrogenlike donor in $CuInSe_2$ is expected at 7 meV and in $CuGaSe_2$ at 13 meV from the conduction band). Thus, the shallower donor in $CuInSe_2$ (compared to the donor in $CuGaSe_2$) makes it more difficult to clearly resolve the switch from the DA to an FB transition. This change between different recombination mechanisms occurs at the same temperature for the DA1 and DA2 transitions [19,20,28], indicating that both transitions start from the same shallow defect, which then becomes ionized as the
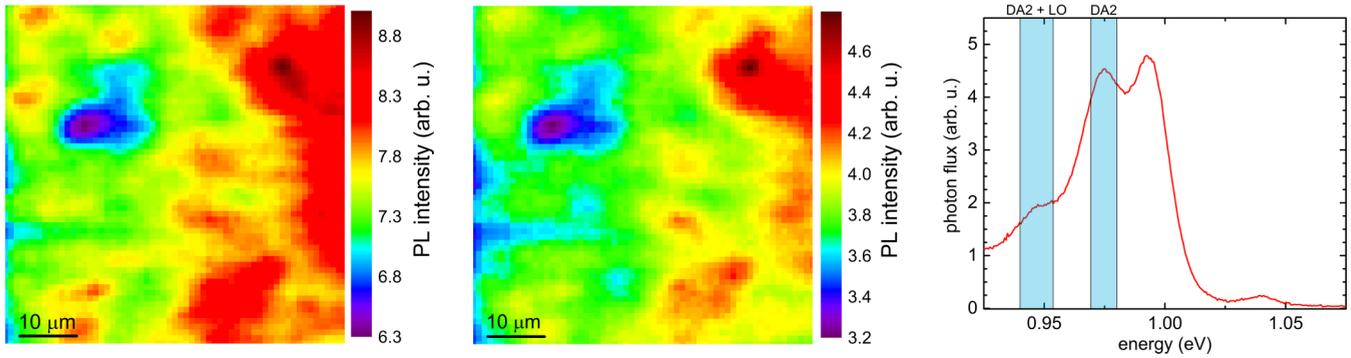
FIG. 2. Spatially resolved maps of low-temperature PL of the DA2 transition (left) and the third transition, labeled DA2+LO (center), in epitaxial CuInSe$_2$. The corresponding energy ranges are marked on the spectrum (right). The third transition is spatially highly correlated with the DA2 in all CuInSe$_2$ and most CuGaSe$_2$ samples, while in some CuGaSe$_2$ it was found to anticorrelate with the DA2 transition. This indicates that the third transition is in most cases a phonon replica of the DA2; in some CuGaSe$_2$ samples it is an independent DA3 transition.

temperature increases. Thus we conclude that the DA1 and DA2 transitions involve the same shallow donor (D1) with an ionization energy of about 10 meV in CuInSe$_2$ and CuGaSe$_2$. This estimate is based on the energy difference between the DA and FB transition plus an estimation of the Coulomb energy involved in the DA transition. This ionization energy is of the order of the Urbach energy of the band tails in epitaxial and polycrystalline ternary films [15]. It can therefore be considered questionable to attribute this energy to a distinct defect. However, in CuGaSe$_2$ we observe clearly separate peaks for the DA transition and the corresponding free-to-bound transition between the conduction band and the A1 and A2 acceptor [19]. We therefore argue that a model with a well-defined defect level is appropriate.

The energetic difference between all three DA-related peaks is in both materials close to the LO phonon energy: about 34 meV in CuGaSe$_2$ [57–59] and 29 meV in CuInSe$_2$ [59,60]. Therefore, it has to be verified whether the observed transitions are independent of each other or whether one is a phonon replica of the other. The ratio between DA1 and DA2 depends on the amount of Cu excess during growth, with DA2 always dominating with higher Cu excess (see Fig. 1). If DA2 was a phonon replica of DA1, the fact that the intensity ratio of the two peaks depends on the amount of Cu excess could only be explained by a change in the Huang-Rhys factor with Cu excess. (The Huang-Rhys factor describes the electron-phonon coupling; for a discussion see Appendix A or the review in, e.g., Ref. [61].) Since the result of a Cu-rich growth process is always stoichiometric chalcopyrite (plus a Cu selenide secondary phase) [12,14], a dramatic change in the electron-phonon coupling with different Cu excess seems highly unlikely, and we identify DA1 and DA2 as two independent transitions.

To obtain information on the energies of these defects, we analyze energies of the FB transitions [19] and the quenching behavior of the DA transitions [20] in combination with the energies of the DA transitions [28]. We can derive the approximate defect ionization energies: about 10 meV for the donor in CuInSe$_2$ and CuGaSe$_2$, 40 and 60 meV for the acceptors A1 and A2 in CuInSe$_2$, and 60 and 100 meV for A1 and A2 in CuGaSe$_2$. The defects in CuGaSe$_2$ are somewhat deeper than in CuInSe$_2$, as one would expect from the hydrogen

model taking the larger effective mass of CuGaSe$_2$ [54] into account. Since these are still shallow defects, they are likely hydrogenlike defects [55] or perturbed host states [62] which do not show significant lattice relaxation, and thus the PL peak maxima are zero-phonon lines and the defect energies derived from them are the same as the thermal ionization energies. This is supported by fitting the observed transitions with a phonon-coupling model (see Fig. 3 and discussion below), which indicates the DA2 transition as the zero-phonon line. The hydrogenlike nature of the shallow defects was additionally confirmed by pressure [63] and polarization [64,65] dependent measurements. The DA1 and the DA2 transitions are observed to shift continuously in Cu(In, Ga)Se$_2$ with increasing Ga content [16,66,67]. It is thus likely that the shallow levels in CuInSe$_2$ and in CuGaSe$_2$ are caused by the same defects. We observe these two transitions DA1 and DA2 in all epitaxial and polycrystalline CuInSe$_2$ and CuGaSe$_2$ films grown under Cu excess. Also, the dependence of the relative intensities on the amount of Cu excess is always observed: higher DA1 at low Cu excess and dominating DA2 at Cu excess above about Cu/III = 1.2. We conclude that Cu-rich CuInSe$_2$ and CuGaSe$_2$ contain the same shallow donor D1 and at least two shallow acceptors A1 and A2. The defects and their energies are summarized in Fig. 8 and Table I. These two shallow acceptors are the ones which are responsible for the p-type character observed in CuInSe$_2$, when it's Cu rich, and in CuGaSe$_2$ of any composition [68].

B. A third shallow acceptor

In both CuInSe$_2$ and CuGaSe$_2$ a third near-band-edge PL transition is observed with a DA-like behavior, which is always lower in intensity than the DA2 and could thus potentially represent a phonon replica of the DA2 transition. If this is the case, then the spatial correlation between these two transitions should be very high. This is in fact observed in most cases, as seen in Fig. 2 for epitaxial CuInSe$_2$ films and in Ref. [67] for polycrystalline CuInSe$_2$. The correlation is already obvious by looking at the PL maps. The cross-correlation coefficient is calculated according to Eq. (B1) in Appendix B and is 0.97. A high correlation between DA2 and the third transition was found in all investigated
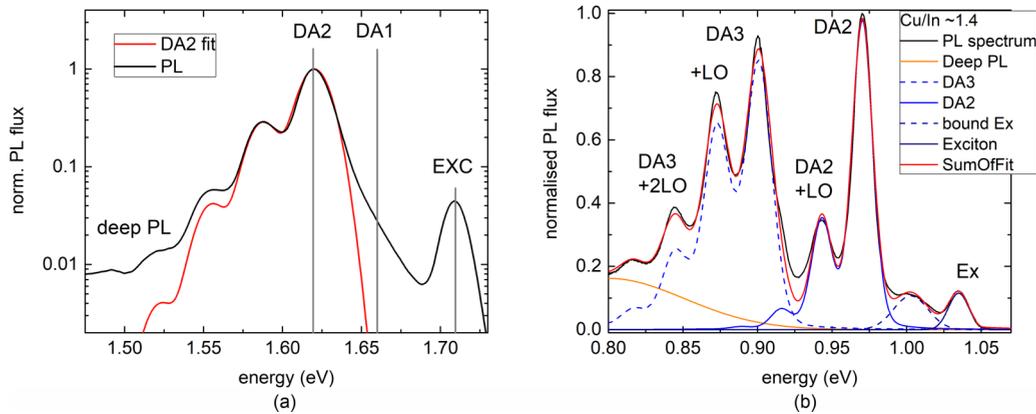
FIG. 3. Low-temperature PL of an epitaxial CuGaSe$_2$ (a) and a polycrystalline CuInSe$_2$ film (b). The CuGaSe$_2$ film (a) was grown under high Cu excess and low Se supply. The third peak at 1.58 eV can be fitted in this case as a phonon replica with a phonon energy of 33 meV, a Huang-Rhys factor of 0.3, and a Gaussian broadening of 22 meV. The CuInSe$_2$ film (b) was grown under high Cu excess and under high Se supply and shows both the DA2 and the DA3 transition with their phonon replicas. The transition at about 0.94 eV is clearly a phonon replica of the DA2. Fits are with a phonon energy of 28 meV, a Huang-Rhys factor of 0.75 for the DA3 transition and of 0.35 for the DA2 transition, and a Gaussian broadening of 19 meV for DA3 and of 16 meV for DA2. This indicates that we do observe a third acceptor in CuInSe$_2$ under Se-rich conditions.

CuInSe$_2$ samples, independent of their Cu content or their polycrystalline or epitaxial nature [67]. Furthermore, in case the third transition is a phonon replica of the DA2 transition, the peak positions and intensities of the transition and its phonon replica should be well modeled by a spectrum of Poisson-distributed amplitudes of phonon replicas according to Eq. (A1) in Appendix A. This is achieved in most CuInSe$_2$ and CuGaSe$_2$ samples with very similar Huang-Rhys factors of around 0.3, as shown in Fig. 3. The low Huang-Rhys factor confirms again that the structural relaxation of A2 upon charge change is low and that A2 is in fact a hydrogenlike defect. Furthermore, these fits show that the third near-edge transition (DA3 or DA2-LO) is, in most cases, a phonon replica of DA2. However, in the case of epitaxial CuGaSe$_2$, grown under rather low Se supply and under low Cu excess, it was observed by spatially resolved cathodoluminescence [69] and photoluminescence [70] that the DA3 transition and the DA2 transition are almost anticorrelated. Thus, it can be concluded that the DA3 transition in CuGaSe$_2$ grown under low Cu excess and under a low Se supply represents an independent transition. It should be noted that the CuInSe$_2$ film in Fig. 2 is grown under very similar conditions and shows a strong spatial correlation between the DA2 and the third transition.

Thus, in most CuInSe$_2$ and CuGaSe$_2$ films the third transition is a phonon replica of the DA2. However, in CuGaSe$_2$ grown under low Cu excess and low Se supply this third transition is independent. Since it shows the same energy shift with temperature and a similar shift with intensity as the DA2 [28] it was concluded that this third luminescence transition starts from the same shallow donor and thus introduces a third acceptor at about 130 meV above the valence band. In the past we had attributed the third transition in CuInSe$_2$ at around 0.94 eV also to an independent DA3 transition [28,66]. This was purely based on the similarity of the PL spectra and their compositional dependence between CuInSe$_2$ and CuGaSe$_2$. This attribution cannot be held up in view of the results shown in Ref. [67] and Fig. 2. In fact, it has been argued that it

is difficult to attribute the third acceptor in CuInSe$_2$ based on defect calculations [24]. It should be noted that in those CuGaSe$_2$ films where the third transition is observed as a spatially independent DA3 transition [69,70], it occurs only in very limited and separated spots about 1 μm across. Because of its unusual behavior we label it A3x (see Fig. 8 and Table I).

In the literature on CuInSe$_2$, another PL transition has been observed at an energy of 0.90 eV, which has been attributed to a DA transition in thin films [18,33,71] or to an FB in single crystals [72,73]. We never observe this transition in our epitaxial films grown by MOVPE under a rather low Se supply (see Fig. 1); we will discuss the reasons below in Sec. V. However, in polycrystalline films grown by thermal coevaporation under high Se supply on Mo-covered glass we do observe this transition [Fig. 3(b)] [67]. Again, the phonon replica of this transition is clearly visible. The fit to a Huang-Rhys model indicates that the transition at 0.90 eV is, in fact, the zero-phonon line. The Huang-Rhys factor is higher for the transition at 0.9 eV than for the DA2 transition, which is expected for a deeper defect. With increasing excitation intensity at low temperatures, the transition at 0.9 eV shows a small but clear blueshift of 0.5 meV/decade, identifying it as a DA transition in these thin films. With increasing temperature this transition shows a slight blueshift that is completely parallel to the blueshift of the DA2 transition [67]. This blueshift is more than the expected blueshift of a DA transition of the order of kT; we therefore interpret this blueshift as the switch from a DA to an FB transition, the same as previously observed for the DA1 and DA2 transition in CuInSe$_2$ [20]. Since this change happens at the same temperature, the donor which becomes empty at this temperature is likely the same. From the energy distance between FB2 and FB3, as well as from analyzing the quenching behavior, we find an energy of around 135 meV for the third acceptor (A3) in CuInSe$_2$ [67]. Because of the unusual behavior of the A3x in CuGaSe$_2$, we would not like to claim that the two defects in CuInSe$_2$ and CuGaSe$_2$ are the same.

C. A second shallow donor

Information about majority defect energies can also come from the temperature-dependent carrier concentration obtained by Hall measurements. Measurements of the temperature-dependent carrier concentration by the Hall effect on epitaxial $CuGaSe_2$ films give support for a deeper acceptor with energies similar to the A3x defect [17,69].

While $CuGaSe_2$ is p type in any composition, Cu-poor $CuInSe_2$ was observed to be n type, when there is no Na doping present [68,74] as confirmed by Hall measurements on epitaxial Cu-poor, Na-free $CuInSe_2$ [75]. It is possible to obtain donor energies from the fitting of the temperature-dependent carrier concentrations. These fits indicate that in all Cu-poor $CuInSe_2$ samples the n-type character is mostly due to a shallow donor, which appears to be the same as observed in PL (D1). The donor is strongly compensated by acceptors, which is again in agreement with the interpretation of the PL measurements in Cu-poor $CuInSe_2$. However, to fit the temperature dependence of the carrier concentration in the Hall measurements, the presence of a second, deeper donor (D2) is needed with an activation energy of about 100 meV. Similar conclusions have been made in the past [76–78]. It seems that this donor is not observed in PL. The reason could be that it is a metastable defect that upon illumination disappears or changes its character or energy level [79]. It is not possible to observe this defect by Hall measurements in $CuGaSe_2$, since $CuGaSe_2$ is always p type and we can only extract information about acceptor energies, not about donor energies, from Hall measurements on p-type samples.

III. DEEP DEFECTS

Most PL investigations in the literature on $CuInSe_2$ and $CuGaSe_2$ concentrate on near-band-edge emissions. But in addition to shallow defects, photoluminescence spectroscopy allows us to study deep defects as well. By measuring the PL spectra, like those in Fig. 1, towards lower energies, deep defects can be analyzed.

A. Deep donors in high-Ga Cu(In,Ga)Se$_2$

Most prominently, a broad double peak at 1.1 and 1.25 eV has been observed in Cu-rich $CuGaSe_2$ [80], also shown by the black spectrum in Fig. 4. The near-band-gap emission shows the excitonic luminescence and the DA2 transition, plus several phonon replicas, i.e., the same spectral structure as the Cu-rich $CuGaSe_2$ in Fig. 1 (black curve). The intensity-dependent investigation [80] of the low-temperature PL indicates that the DA2 and both deep transitions involve the same defect that saturates at a certain excitation density. Additionally, from the shift of the peak position with excitation intensity, we can discern the Coulomb energy involved in these donor-acceptor pair transitions, which in turn allows us to discern the defect size [81]. These measurements imply that the shallow defects in both deep transitions have to be acceptors [80]. Therefore the common defect in those three transitions is the A2 acceptor and the two deep transitions involve two deep donor states (labeled DD1 and DD2 in the following). From Fig. 4 we can see that the observed transitions are rather broad. This could be due to a broad
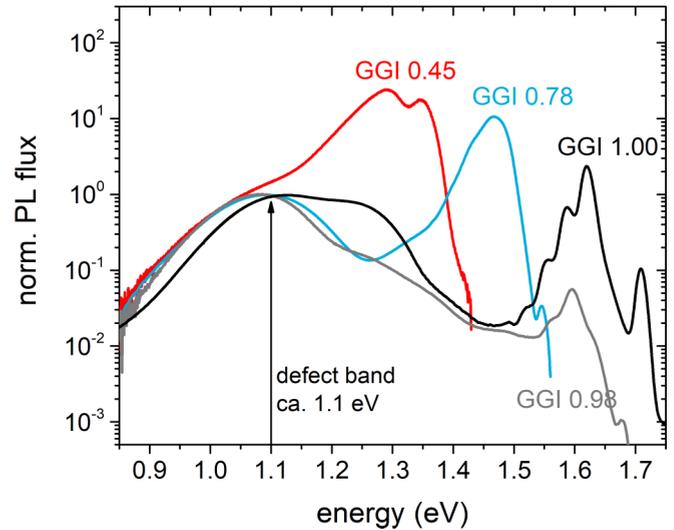
FIG. 4. PL spectra, normalized at 1.1 eV, measured at 10 K for a set of Cu-rich Cu(In, Ga)Se$_2$ epitaxial films on GaAs, with Ga/Ga+In (GGI) ratio varying between 0.45 (red) and 1.0 (black). The highest energy peak in all spectra is the near-band-edge transition, which shifts to lower energies with lower Ga/Ga+In ratio. All films show a deep transition (DD2-A) around 1.1 eV (vertical arrow) that shifts only very little with varying composition and indicates a deep defect at an energy independent of the Ga/Ga+In ratio. Additionally, both high-Ga films also show the DD1-A transition at around 1.25 eV. A similar series with Cu-poor films is shown in Appendix C.

density of states or due to electron-phonon coupling with a rather large Huang-Rhys factor (see Fig. 12 in Appendix A for the relationship between spectral shape and Huang-Rhys factor). In general, deeper defects show a stronger electron-phonon coupling and thus higher Huang-Rhys factor. This is due to the fact that deep defects are more localized, and any change in their charge state thus leads to a significant lattice relaxation (see Appendix A, or, e.g., [82] or [83]). Thus it is expected that the broadening stems from electron-phonon coupling. Since a strong electron-phonon coupling leads to a Franck-Condon shift, it is not possible to derive the defect energy directly from the peak maximum, as we did for shallow defects (We also showed by fitting to Eq. (A1) that the line is in fact the zero phonon line). To determine the defect energy nonetheless, it is necessary to find the zero-phonon line energy from a fit using the Huang-Rhys factor and a one-dimensional configuration coordinate. For a recent summary on phonon coupling of deep defects, see [61] or [84], where also a numerical proof based on *ab initio* calculations is provided that shows that the one-dimensional configuration coordinate is correct, at least under realistic conditions. Unfortunately, the fit is hampered in the case of DD1 and DD2 in $CuGaSe_2$ by the fact that the two transitions overlap. However, upon adding indium to the films, the intensity of the DD1 transition decreases (gray curve in Fig. 4 with only 2% In, which resulted from residuals in the MOVPE reactor). With about 20% In, i.e., with a Ga/Ga+In ratio of ~80% (blue curve in Fig. 4), the DD1 transition disappears completely while the DD2 transition remains essentially unchanged. This transition can then be fitted with a Huang-Rhys model (see, e.g., [61]
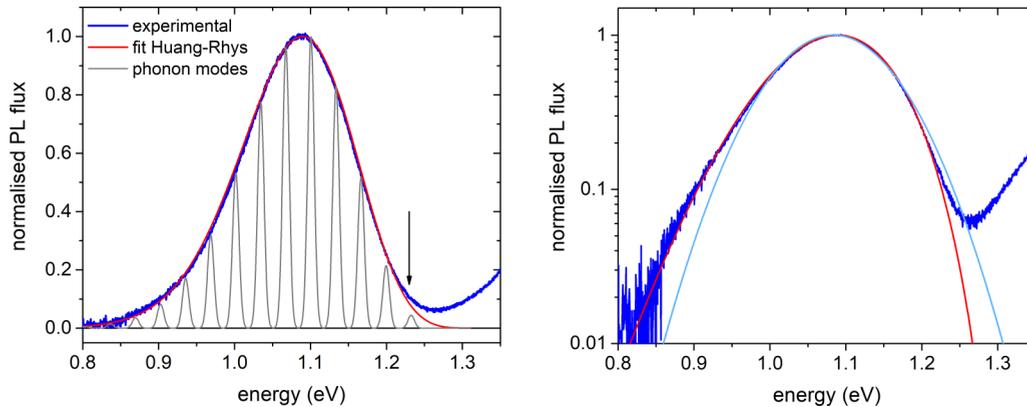
FIG. 5. Linear (left) and logarithmic (right) plot of the measured PL spectrum of the DD2 transition around 1.1 eV (blue curve) at 10 K for an epitaxial Cu(In, Ga)Se$_2$ film with a Ga/Ga+In ratio of 0.8. The linear PL spectrum is shown together with a fit (red) to the Huang-Rhys model of electron-phonon coupling [Eq. (A1)] and a plot (gray) of Eq. (A1) with a reduced Gaussian broadening σ of the individual transitions to demonstrate individual phonon lines. The log plot clearly shows the asymmetric shape typical for lines broadened by electron-phonon interaction (red line), compared to a Gaussian fit (cyan line), indicating that the broadening is, in fact, due to electron-phonon coupling and not to a broad density of states. From the fit the zero-phonon line can be extracted at 1.23 eV, indicated by the black arrow in the left graph.

and Appendix A). Figure 5 shows the experimental curve, together with a fit to Eq. (A1) (in Appendix A) with a phonon energy of 33 meV, a Huang-Rhys factor of 4.6, and a Gaussian broadening of 31 meV. We also present the logarithmic plot in Fig. 5, which clearly shows the asymmetric shape, typical for broadening by the electron-phonon interaction. In contrast, if the broadening of the transition was caused by a broad density of states, a symmetric Gaussian broadening would be expected. Thus, we take the asymmetric shape and the excellent fit to Eq. (A1) as proof that the broadening is due to electron-phonon coupling and not due to a broad density of states. From the fit we can determine the zero-phonon line at 1.23 eV, significantly above the energy of the peak maximum. Taking into account that the transition is between DD2 and the 100-meV-deep A2 and taking into account that the fit in Fig. 5 is done at the lowest excitation intensity possible to minimize the influence of the Coulomb shift indicates that the DD2 has an energy of 1.33 eV above the valence band or about 400 meV below the conduction band. Assuming the same phonon coupling for the DD1 defect, the energetic difference in the peak maximum would correspond to the energetic difference between the zero-phonon lines. This places the DD1 150 meV above DD2, i.e., at 250 meV below the conduction band.

It is interesting to investigate how the two deep defects change when changing the band-gap energy of the Cu(In, Ga)Se$_2$ compound by adding indium. Figure 4 shows the low-temperature PL spectra measured for a series of Cu(In, Ga)Se$_2$ epitaxial films, starting with the pure CuGaSe$_2$ film discussed above, which shows a double peak indicative of the two deep defects DD1 and DD2. When gradually adding indium, the near-band-edge luminescence shifts to lower energies, as expected for the decreasing band gap. The deep defect luminescence, however, stays at an energy of around 1.1 eV, as indicated by the black vertical arrow in Fig. 4. This behavior has been observed for Cu-rich and Cu-poor films. The double character of the peak disappears as soon as more than a few percent of indium is added to CuGaSe$_2$. The reason for the disappearance of the DD1-related transition with addition of indium is not clear. A potential explanation

is discussed below in Sec. V. The remaining luminescence peak has been attributed to the transition between the DD2 defect and the A2 defect. Previous studies [16,67] of the near-band-edge luminescence of Cu(In, Ga)Se$_2$ have shown that the A1 and the A2 defects shift continually in energy between CuInSe$_2$ and CuGaSe$_2$, i.e., the energy of the A2 acceptor involved in the observed deep transition will change by only a few 10 meV, whereas the band gap decreases by about 400 meV, as seen by the luminescence spectra in Fig. 4. Since the luminescence attributed to the DD2-A2 transition stays essentially at the same energy, we can conclude that the DD2 defect stays at the same energy with respect to the A2 defect, i.e., with respect to the valence band. The luminescence merges almost with the near-band-gap luminescence at a Ga/Ga+In ratio of around 0.45 and a band gap near 1.3 eV. In this spectrum, the "deep" transition is visible only as a shoulder (red curve in Fig. 4), indicating that the involved defect is close to the band edge. The band-gap difference between CuInSe$_2$ and CuGaSe$_2$ is almost exclusively due to a shift in the conduction band [85,86]. Thus, when the defect energy with respect to the valence band remains unchanged upon addition of indium to CuGaSe$_2$, as observed for the DD2 defect, it will eventually become shallow and merge with the conduction band at a band edge energy of about 1.3 eV, as depicted in Fig. 6. It has been observed many times that solar cells made from Cu(In, Ga)Se$_2$ exhibit a strong increase in the open-circuit voltage loss when increasing the band gap of the absorber beyond about 1.25 eV [87], approximately coinciding with the band-gap energy below which the deep defect DD2 is shallow. We consider this a strong hint that DD2 is at least partly responsible for the efficiency loss in wide-gap Cu(In, Ga)Se$_2$ solar cells.

B. The "0.8-eV defect"

In the literature, a broad defect at about 800 meV above the valence band has been detected by photocapacitance spectroscopy in Cu-poor Cu(In, Ga)Se$_2$ films with varying Ga content [88]. A corresponding PL emission was observed at
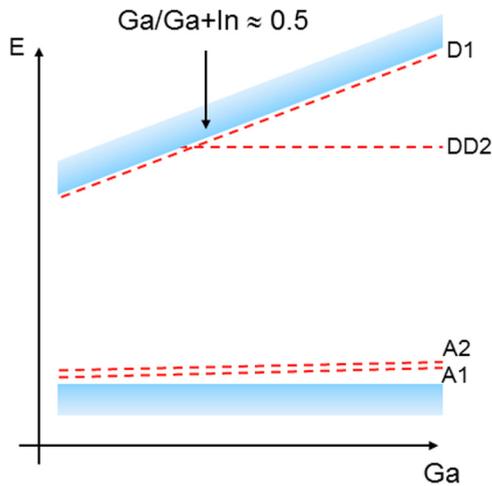
FIG. 6. A schematic diagram of the changes of band and defect energies when moving from $CuInSe_2$ to $CuGaSe_2$. We neglect any change in the energy of the valence-band maximum. The two shallow acceptors A1 and A2 become slightly deeper with increasing gallium. There is always a shallow donor with nearly constant energy distance to the conduction band. The DD2 defect disappears into the conduction band with decreasing Ga content and becomes shallow at a band-gap energy of about 1.3 eV.

low temperatures but not discussed in Ref. [89]. A broad PL emission centered at about 0.8 eV is clearly visible in Fig. 3 of Ref. [89] in $CuInSe_2$ films grown under Cu excess. In Cu-poor $CuInSe_2$ films it was visible only after annealing in air. A similar deep defect transition has been observed [90] by low-temperature PL in standard Cu-poor $Cu(In, Ga)Se_2$ with a Ga/Ga+In ratio of around 30%, albeit with a much narrower luminescence peak width.

We also observe a broad transition with peak energies between 0.7 and 0.8 eV in low-temperature and room temperature PL spectra of epitaxial and polycrystalline $Cu(In, Ga)Se_2$ films. Examples are shown in Fig. 14 in Appendix D. As a trend we observe the transition rather around 0.7 eV in samples with a high Ga/Ga+In ratio and around 0.8 eV in samples with a low Ga/Ga+In ratio. Furthermore, we observe this transition generally in Cu-rich samples and much less in Cu-poor samples. Often, this transition appears simply as an increased background at low energies. This background is seen in all our Cu-rich films and is much lower in Cu-poor samples, see Fig. 7(a). We therefore conclude that the corresponding defect is more prominent in Cu-rich $Cu(In, Ga)Se_2$, as also observed in Ref. [89].

The transition is rather broad in all cases (see Appendix D, Fig. 14). If the broadening was due to electron-phonon interaction, the zero-phonon line would occur at higher energies. The zero-phonon lines can be obtained from a simplified peak fit which describes the peak width, according to Ref. [91]; it would appear 100 meV higher than the peak maximum in this case. However, the peak can be well fitted by a Gaussian shape and shows little asymmetry, which could be a hint that the broadening is actually caused by a broad density of states. This interpretation is supported by the unusual temperature and excitation dependence depicted in Figs. 7(b) and 7(c), which shows the behavior of a Cu-rich epitaxial $CuInSe_2$ film

+++. We discuss it in detail in the next paragraph. In the temperature-dependent series [Fig. 7(b)] the peak at around 0.8 eV is clearly seen between 80 and 140 K, shifting to lower energies with increasing temperature: from 0.83 eV at 60 K to 0.76 eV at 140 K. Since the transition shifts red with increasing temperature, it can be excluded that we observe the change from a donor-acceptor pair transition to a free-to-bound transition. We therefore interpret this transition as a free-to-bound transition, originating from a broad deep defect. Whether this defect state is donorlike or acceptorlike cannot be decided based on these measurements. We propose an interpretation in Sec. V based on the correlation with calculated defect levels.

As already observed by photocapacitance spectroscopy measurements in the literature [88], the transition energy in PL remains around 0.8 eV independent of the Ga content of the sample (see Fig. 14, Appendix D). If this energy would be observed with respect to the conduction band, the defect state would be a state close to the valence band in $CuInSe_2$ but would shift higher into the gap as the Ga content increases. It is unlikely that a defect close in energy to the valence band shifts with the conduction band. It is much more likely that the transition is between the defect and the valence band. This would place the defect at 200 meV from the conduction band in $CuInSe_2$ and would move it further away from the conduction band with increasing Ga content. The defect would thus stay at a constant energy with respect to the valence band, very much like the DD2 defect (see Fig. 6). We thus believe this to be the most likely interpretation of the observed transition: a defect with a broad density of states centered at around 0.8 eV from the valence band.

The free-to-bound transition in $CuInSe_2$ is broad and shifts in an unusual way with temperature and intensity [Figs. 7(b) and 7(c), summarized in Fig. 7(d). It blueshifts with increasing intensity with a very high rate of 20 meV/decade [Fig. 7(c)]. Such shifts are observed for transitions in compensated semiconductors, but this sample is not compensated, as can be seen from the narrow near-band-edge emissions at low temperature in Fig. 7(b). The redshift with increasing temperature is unusual for a free-to-bound (or a donor-acceptor) pair transition. The most natural explanation of these shifts is a broad density of states or a collection of different states [92]. Both with increasing temperature or with decreasing intensity, the minority quasi-Fermi level will move to lower energies within or near the defect distribution. Thus the average energy of occupied states, which are available for the radiative transition, will shift to lower values and thus the luminescence maximum. With a lower quasi-Fermi level also the intensity of the transition should be lower. This is exactly what we observe, see Fig. 7(d): for both the intensity dependence and the temperature dependence, the energy of the transition shifts higher with higher PL flux, i.e., higher quasi-Fermi level. The shift would only be observed when states are available at different energies, i.e., with a broad density of states for this defect. This interpretation agrees with the interpretation of the previous photocapacitance measurements, which were fitted with a Gaussian-shaped defect density of states with a FWHM of about 200 meV [88]. We thus attribute the broad transition at around 0.8 eV to a broad deep state, which we label DS.
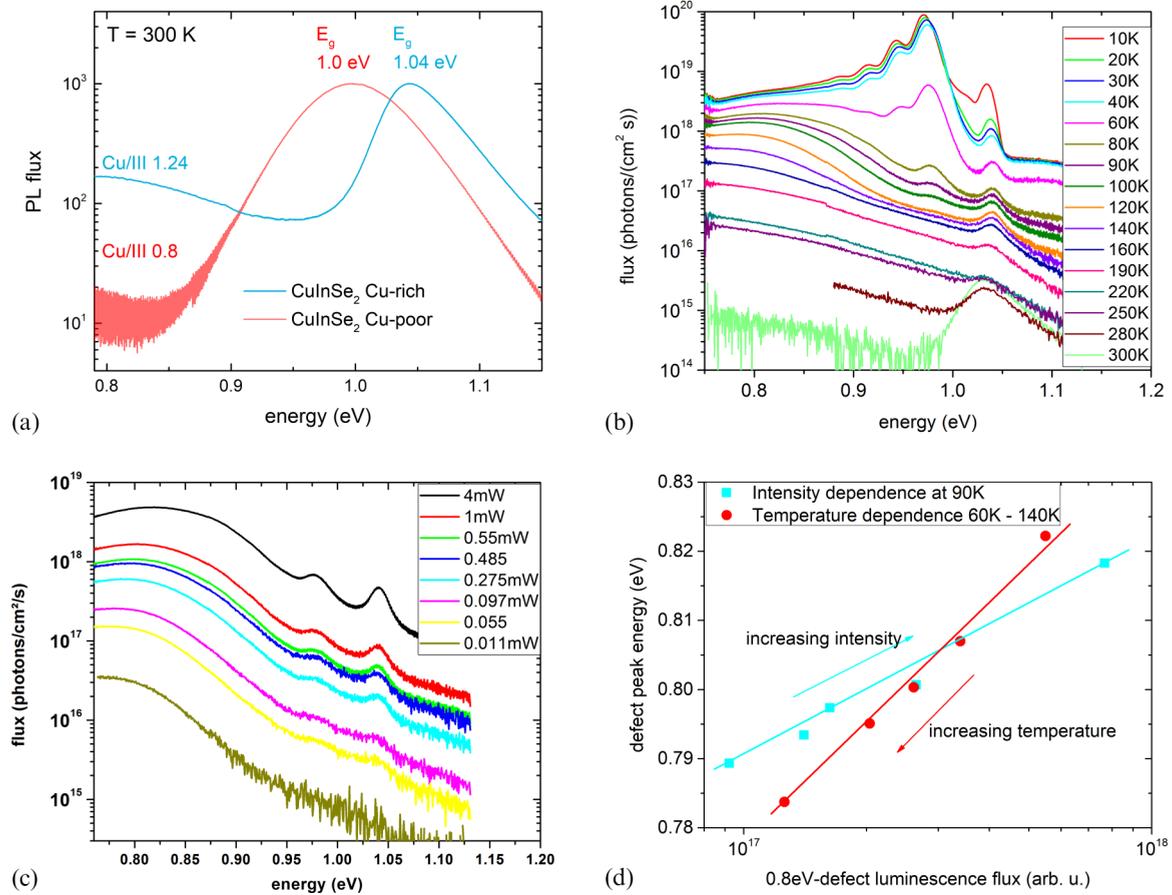
FIG. 7. The 0.8-eV transition in PL. (a) Typical room temperature PL spectra of a Cu-rich and a Cu-poor epitaxial $CuInSe_2$ sample indicating the deep luminescence in Cu-rich samples that is not present in the Cu-poor sample (measured at 20 mW excitation). (b) Temperature dependence of the PL of a Cu-rich epitaxial $CuInSe_2$ sample at 1 mW excitation, clearly indicating the transition at around 0.8 eV but only at intermediate temperatures. (c) Excitation dependence of the PL spectra of the same sample at 90 K. (d) Correlation between PL flux and energy position from parts (b) and (c). With increasing excitation intensity or decreasing temperature, the quasi-Fermi-level shifts higher within the broad density of states, increasing both intensity and maximum energy of the transition. Thus these measurements indicate a broad density of states centered at around 800 meV, likely above the valence band.

TABLE I. Summary of defect energies obtained from our PL and Hall measurements. Shallow donors and acceptors are labeled D and A, respectively, deep donors are labeled DD, and deep gap states, which are not identified as a donor or acceptor, are labeled DS. To compare with electrical measurements from the literature, we add the labels used in Ref. [93]. The assignment is based on comparison with five recent theoretical studies as described in Sec. V. We are less confident with the assignments marked with a "?"

Defect	$CuInSe_2$		$CuGaSe_2$		Label in Ref. [93]	Assignment
	Energy (meV)	wrt[a]	Energy (meV)	wrt[a]		
A1	40	VB	60	VB		V_{Cu}
A2	60	VB	100	VB	E6	$Cu_{III}^{0/-1}$
A3	135	VB				$V_{In}^{0/-1}$?
A3x			130	VB	E7	
D1	10	CB	10	CB		Cu_i, In_{Cu}
D2	100	CB	Likely similar, but not detectable			V_{Se}-V_{Cu}?
DD2	Shallow		400	CB	E1($CuGaSe_2$), E3	Ga_{Cu}
DD1	–		250	CB		$Ga_{Cu}^{0/+1\ or\ +2}$?
DS	~800 broad	VB	~700 broad	VB	E2, E8	$Cu_{III}^{-1/-2}$?

[a]with respect to (wrt).
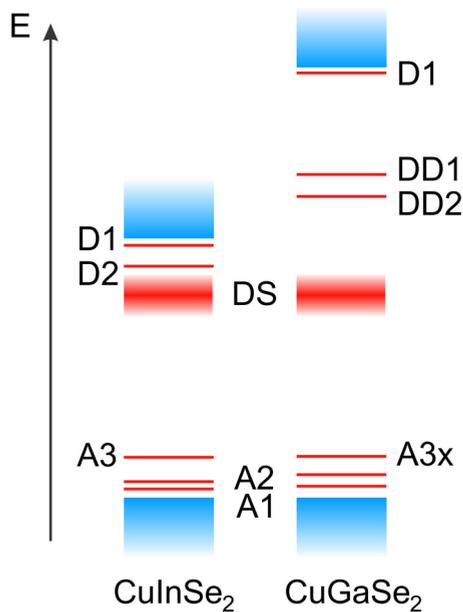
FIG. 8. Summary of defect levels for which experimental evidence has been discussed here. Shallow donors and acceptors are labeled D and A, respectively, deep donors are labeled DD, and deep gap states, which are not identified as a donor or acceptor, are labeled DS. See also Table I. It should be noted that all defects are deduced from PL measurements, besides D2 which is deduced from Hall measurements.

This defect appears to be ubiquitous: it was first observed by photocapacitance spectroscopy in Cu-poor films, independent of the Ga content [88]. In our PL investigations, as well as in previous PL measurements [89], we find it more strongly in Cu-rich films than in Cu-poor films, also independent of the Ga content. The question then arises as to why it was hardly ever observed in PL spectra [90]. A possible answer becomes obvious from the temperature dependence of this transition, depicted in Fig. 7(b). The peak appears only as a flat background at low temperatures, becomes visible at intermediate temperatures, and then shifts to lower energies (and out of the measurement range of many setups) at higher temperatures.

Summarizing, we observe two different types of deep defects (see also Fig. 8 and Table I): (i) The deep double donor DD2 and DD1 at 1.33 and about 1.5 eV above the valence band, which are only visible for high Ga contents. DD1 disappears upon indium addition and DD2 becomes shallow for Ga/Ga+In smaller than 0.45. (ii) The broad defect state DS at about 800 meV above the valence band. They are summarized in Fig. 8 and Table I.

IV. COMPARISON WITH OTHER EXPERIMENTAL METHODS

Besides the PL and Hall measurements discussed here, a range of other methods have been applied to study defects in Cu(In, Ga)Se$_2$. We first discuss capacitance- and photocurrent-based methods, which indicate the electronic energy levels of defects. Next, we discuss experimental methods that reveal the physicochemical nature of defects, such as

neutron and x-ray diffraction and positron annihilation, which we summarize as structural methods below.

A. Capacitance and transport measurements

The energy of defect states is also determined from electrical measurements. These methods are based on capacitance measurements, like admittance spectroscopy (AS) or deep-level transient spectroscopy (DLTS), or on transient transport measurements, like photoinduced current transient spectroscopy (PICT) and modulated photocurrent spectroscopy (MPC). These methods all rely on the temperature dependence of their responses to extract defect energies. In the case of deep defects that experience a Franck-Condon shift, the extracted defect energies would correspond to the thermal energies, i.e., the energetic difference E_0 between the minima in the configuration diagram (see Fig. 11 in Appendix A or, e.g., [61]). Since capacitance measurements have to be done on finished devices which consist of many layers and interfaces, their interpretation can be difficult. Many effects can contribute to the measured capacitance that are not related to bulk defect energies: interfaces [94–96], the presence of the buffer layer [97], interface defects [98], or transport freezeout [99]. MPC and PICT are not hampered by interface and buffer influences, but there is some disagreement on how to correctly analyze MPC measurements [100], which would have some influence on the determined defect energies. A recurring observation in these thermal methods is that the defect energies differ between samples. To decide whether the various energies originate from the same defect, usually a Meyer-Neldel plot [101] is made of the data obtained from the Arrhenius fit of the response frequency, which relates essentially the prefactor, dependent on the capture cross section, to the activation energy. Signals originating from the same defect are supposed to lie on a straight line, because the activation can be considered a multiphonon process, the entropy of which has to be taken into account in the free energy of the excitation process [102]. Thus, why the same defect should lie on a Meyer-Neldel line can be explained. However, the question remains open why the same defect occurs at different energies in different samples, particularly since in PL the scatter of the energies between different samples is smaller than the peak width. A possible explanation for the observation of differences in the defect energy in capacitance methods could be a Poole-Frenkel effect because of the high electric field within the space-charge region, which can easily be different between different samples. However, in the transient transport methods, the applied fields are much lower and cannot cause any significant energy reduction by the Poole-Frenkel effect and thus cannot explain the scatter in emission energies observed. But a Meyer-Neldel behavior is also observed when two thermally activated processes contribute to the measured quantity [103,104]. In the case of capacitance or transport methods discussed above, this could be, e.g., the emission from the defect and the transport over grain boundaries. The measured activation energy in each case would lie between the activation energies of the two processes and closer to that which contributes more to the measured quantity [103]. The band bending at grain boundaries can be very different, even within one sample [105]. If we assume a

small contribution of the transport across the grain boundaries on the measured activation energies, the measured activation energies would still be close to the defect emission energy but could, in fact, vary from sample to sample. This could be another explanation of the observed Meyer-Neldel behavior.

One of the first investigations of capacitance spectroscopy in Cu(In, Ga)Se$_2$ solar cells [98] found two defects, labeled N1 and N2 at 120- and 280-meV activation energy, respectively. The N2 was identified as a bulk defect and is still today considered a bulk defect by most authors. The N1 was identified with an interface defect in this early paper [98]. Meanwhile, admittance signals in the energy range around 100 meV have been attributed to a bulk defect [106], to mobility freezeout [99], to a barrier at the back contact [95], or to a barrier at the front side [96]. It is likely that signals observed in the energy range of the N1 defect can originate from a variety of causes [107]. For sure, from our PL measurements we can conclude that acceptor-type bulk defects exist in Cu(In, Ga)Se$_2$ in the energy range between 40 and 130 meV. Thus, a certain contribution of a bulk defect to the N1 appears necessary.

The ambiguity between interface and bulk effects can be solved by applying photocurrent methods. A summary of a comprehensive investigation of defects in Cu(In, Ga)Se$_2$ based on capacitance as well as on transient transport methods can be found in Ref. [93]. The observed energy range of some of these defects clearly correlates with the energies observed in PL and Hall. In Table I we relate the defects found in PL and Hall to the labels given in Ref. [93]. A discussion on why we do not see certain defects is given in Appendix E.

While we believe that those defects mentioned in Table I can be correlated with our PL and Hall results, it should be noted that it is sometimes even difficult to correlate capacitance and/or electric transport measurements on different samples. The difficulties are discussed, e.g., in Refs. [108] and [109], which attempt to correlate the defects found in their studies with those found in previous publications. Because of the difficulties correlating different defect signatures between different samples and particularly because of the difficulties to determine an exact defect energy, for our defect model we concentrate on the results from PL and Hall measurements.

B. Structural measurements

The optical and electrical measurements discussed so far give insight into the electronic states associated with defects in these crystals. To gain insight into the physicochemical structure of these defects, other methods are needed. A classic tool to learn about the local symmetry and the charge state of defects is electron paramagnetic (or spin) resonance EPR or ESR [110,111]. However, no EPR signal in Cu(In, Ga)Se$_2$ could so far be surely identified with a native defect [112]. One narrow, but isotropic signal with a *g* value close to that of the free electron is sometimes assigned to the Se vacancy [112,113]. Other studies attribute the signals rather to impurities or oxidized Cu [114,115] or to aggregates of defects, which cannot be clearly defined [116,117]. Thus EPR measurements so far cannot be used to identify defect structures.

Vacancy-type defects can be studied by positron annihilation. Stoichiometric single crystals of CuInSe$_2$ showed double-vacancy defects, but only after irradiation [118]. Measurements on Cu-poor Cu(In, Ga)Se$_2$ polycrystalline films indicate the Cu vacancy as the main vacancy defect based on the Doppler broadening, i.e., on the energy spectrum of the emitted photons [119]. An analysis of positron annihilation in epitaxial CuInSe$_2$ films based on positron lifetimes concluded Cu vacancy as the main vacancy defect in CuInSe$_2$ grown under Cu excess and the Cu-Se double vacancy as the main vacancy defect in Cu-poor films [89]. Similar results were obtained on epitaxial CuInSe$_2$ and CuGaSe$_2$ films based on the energy spectrum of the emitted photons [120]: in Cu-poor CuInSe$_2$ the double vacancy dominates, whereas in stoichiometric CuInSe$_2$ and CuInSe$_2$ grown under Cu excess the Cu vacancy dominates. In contrast, in CuGaSe$_2$ the double vacancy was observed for all compositions. The double vacancy was also found in polycrystalline CuInSe$_2$ [121] and CuGaSe$_2$ films [122]. Mono- and double vacancies were found in polycrystalline Cu(In, Ga)Se$_2$ films [123], particularly under low Se pressure [124]. In several polycrystalline film studies [121,123], large vacancy clusters were also found. Concerning point defects, it can be concluded that there is ample evidence for Cu vacancies and Cu-Se double vacancies from positron annihilation.

Cation-related point defects have been studied by neutron diffraction on CuInSe$_2$ powders [22]. High concentrations of several 10^{20} cm^{-3} were found for the Cu vacancy and both antisite defects Cu$_{In}$ and In$_{Cu}$ in Cu-poor material. In material grown under Cu excess, only the Cu$_{In}$ antisite was found in high concentration. This defect was observed in very similar concentrations in Cu-poor and Cu-rich material. In Cu-poor material the two antisite defects are expected to almost cancel out in terms of composition and in terms of electrical activity. The powders were crystallized over weeks, meaning that this material is as close to thermal equilibrium as possible. It is unlikely that films grown over hours, like the polycrystalline and epitaxial films investigated by PL and discussed above, would have lower defect concentrations. Cu-poor CuGaSe$_2$ powders were studied by neutron and anomalous x-ray diffraction [125]. Since the neutron scattering lengths of Cu and Ga are rather similar, model structures have to be assumed for the point defects. As the most likely scenario, a situation emerged with a high concentration (in the 10% range) of Cu vacancies and Ga interstitial sites, together with about 5% of antisites. However, the models considered for the analysis were only those, where a balance between the Cu vacancy concentration and the Ga interstitial concentration was assumed, together with a balance between the antisites. Furthermore, density functional theory (DFT) calculations show that the Ga$_{Cu}$ antisite can form a DX center, where the Ga moves towards an interstitial site [126,127]. Since the formation energy of the III interstitial defect is very comparable in CuInSe$_2$ and CuGaSe$_2$, according to hybrid functional calculations [127], and since no In interstitials were observed in CuInSe$_2$ [22], it appears unlikely that the high concentration of Ga interstitials is the only explanation for the observed diffraction patterns. Thus, in both CIS and CuGaSe$_2$ Cu vacancies were found in Cu-poor material, together with both antisites. Cu-rich CuInSe$_2$ contains only the Cu$_{In}$ antisite in high concentrations.

V. COMPARISON WITH THEORY

Finally, we would like to correlate the observed electronic levels with physicochemical defect structures. Since, in general, the low-temperature PL spectra are very similar between epitaxial and polycrystalline samples (see, e.g., [16]) grown on very different substrates, with and without alkali content and using very different growth methods, it is safe to assume that the defect signatures listed in Table I are due to native defects. A clue to the defect nature can be obtained from the composition dependence of a specific defect, e.g., it is highly unlikely that the density of Cu vacancies V_{Cu} increases with increasing Cu pressure during growth. However, such considerations have to be used with great care, since in ternary compounds, controlling only one of the constituents is not enough [128], as has been observed in $CuInSe_2$, where a change in Se flux led to a change in Cu/In ratio in the films although the Cu and In fluxes were not changed [129]. Thus, to obtain insight into the physicochemical nature of the observed energy levels it is indispensable to compare with defect predictions from theory. The first comprehensive defect studies were based on density functional theory in the LDA (local density approximation) approach [130–132]. These early theoretical calculations showed no obvious correlation of the obtained defect energies with the experimental findings, but they paved the way for further investigations. Since then theoretical methods have been greatly improved and, since the development of hybrid functionals [133], much more precise predictions of the electronic structure of semiconductors are possible [134].

In recent years a number of new defect calculations have been performed for $CuInSe_2$ based on hybrid functionals [24,127,135–137]. An overview of the predicted defect energies is given in Fig. 9. These defect energies are obtained from the crossover points of the formation energies of different charge states of the defects in dependence on the Fermi energy, i.e., the Fermi energy positions where the defect changes its charge state. They relate thus to the thermal energies E_0 (see Appendix A, Fig. 11). Since the calculated band-gap energies are not the same in these studies, we present the defects at energies relative to the closest band edge. Shallow defects, which are resonant with the band in the calculations, are depicted 30 meV away from the valence band for acceptors and 10 meV away from the conduction band for donors, close to the levels of hydrogenlike defects in $CuInSe_2$. It should be noted that not all authors calculated all possible defects. The figure shows for each study all calculated defects. Compared to $CuInSe_2$, very few defect calculations with hybrid functionals are available for $CuGaSe_2$; Pohl et al. consider $CuGaSe_2$ in the same study as $CuInSe_2$ [127]. Another study of both materials considered all defects in the metal sublattice [138] and found them all to be resonant with the bands, i.e., they would appear as shallow defects. However, a later study by the same authors for $CuInSe_2$ only [137] discussed an "erroneous charge correction" in the previous paper. The defect energies for $CuInSe_2$ were corrected and are used in Fig. 9. Since no corrections are available for the earlier $CuGaSe_2$ results [138], we do not consider them here. A recent paper [139] uses an improved hybrid functional that determines the parameters of the functional (mixing parameter and screening
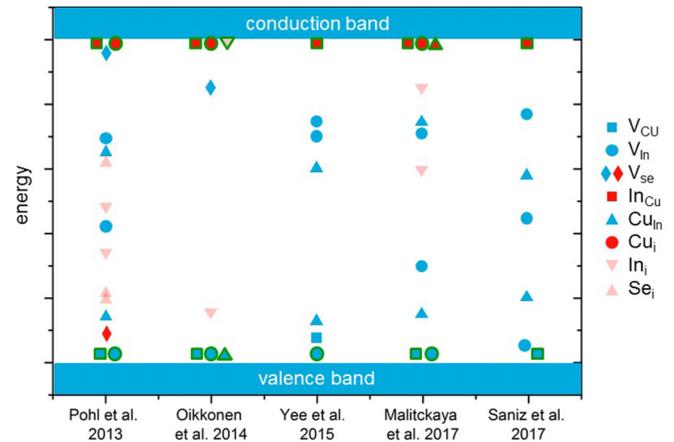
FIG. 9. Defect energies in $CuInSe_2$ obtained from hybrid functional DFT calculations. Acceptors are depicted in blue, donors in red. Shallow defects are shown with a green outline. Light color is used for those defects with a high formation energy (see text for a discussion). The data is from Pohl and Albe [127], Oikkonen et al. [135], Yee et al. [136], Malitckaya et al. [24], and Saniz et al. [137]. The error of the calculated energies is about one minor tick distance. Comparing the accumulated theoretical defect energies with the experimental defects in Fig. 8 leads to the attributions given in Table I.

parameter) not only by fitting to the experimental band gaps, but also observing Koopmans' theorem, i.e., requiring a linear behavior of the total energy with fractional occupation [140]. On the other hand, a smaller supercell was used. The energies of the metal antisites were calculated. The energy level for the first charge transition of Ga_{Cu} is found to be similar to the results of Pohl et al. But the first charge state of Cu_{Ga} is found to be considerably deeper in the gap than in the study by Pohl et al. However, the calculated energy of this level is particularly dependent on the supercell size [141]. We therefore rely mostly on the results by Pohl et al. to compare with our experimental results in $CuGaSe_2$.

Pohl et al. [127] are the only ones who consider a selenium interstitial Se_i. Its formation energy is around 3 eV or higher, even for Se-rich compositions. The indium interstitial In_i is calculated by Pohl and Albe [127], Oikkonen et al. [135], and Malitckaya et al. [24]. Although they report quite different energy levels for this defect, they all find high formation energies, similar to those of Se_i. It is therefore unlikely that these defects are formed, except under some extreme nonequilibrium conditions; they will thus be neglected in the following discussion. Considering the defects with lower formation energies, an amazing agreement concerning the defect levels can be seen from Fig. 9, although all these studies used somewhat different parameters for the functional and different charge correction schemes. It should be noted that the accuracy of the calculated energy of a defect level is about 0.1 eV [24,135].

A. Shallow defects

All five studies find two more or less shallow acceptors, with low formation energy (around 1 eV or below): V_{Cu} and Cu_{In}. The results for $CuGaSe_2$ are similar for V_{Cu} and Cu_{Ga}

[127]. It can thus be concluded that these two are the two acceptors always observed in near-band-edge photoluminescence: A1 and A2. The PL transition related to A1 is visible only for low Cu excess, see Fig. 1. We therefore attribute A1 to the Cu vacancy. The DA2 transition becomes dominant in all samples with increasing Cu excess. Therefore we assign the A2 to the Cu_{III} antisite (III = In or Ga). This is also in agreement with the fact that the Cu_{In} antisite was found to be the dominating defect in Cu-rich $CuInSe_2$ by neutron scattering [22].

All five theory studies find a third shallow acceptor: V_{In} or V_{Ga} (collectively labeled V_{III}). However, the formation energy of this defect is rather high, 2–2.5 eV in the best case. It can be noted from [127] that the lowest formation energy of the V_{III} defects is found under Se-rich conditions. We detect the A3 only in $CuInSe_2$ and low-Ga $Cu(In, Ga)Se_2$ polycrystalline films grown under Se-rich conditions [Fig. 3(b)] [67]. In epitaxial $CuInSe_2$ samples grown by MOVPE with a rather low Se supply, there is no DA3 at all; the third peak, previously erroneously labeled DA3, is a phonon replica of the DA2, as we have shown above in Sec. II B. Our epitaxial samples are grown by MOVPE, where the Se is available only after the precursor is decomposed at growth temperature. In particular, during cooldown Se can be supplied in the coevaporation process but not in the MOVPE process. It is therefore very likely that the equivalent Se pressure is much lower in the MOVPE than in the coevaporation process used for growth of the polycrystalline films. This assumption agrees with the observation that the DA3 transition appears also in polycrystalline samples only when grown with a high Se supply. We therefore attribute the A3 acceptor in $CuInSe_2$ to the indium vacancy. The A3x acceptor in $CuGaSe_2$ behaves differently: the corresponding DA3 transition occurs only for slightly Cu-rich films. In films with higher Cu excess, this transition is a phonon replica of the DA2 [Fig. 3(a)]. Furthermore, it appears only in small spots [69]. Therefore we do not propose that the A3x defect in $CuGaSe_2$ is the gallium vacancy. It could possibly be a defect complex, but theoretical predictions on energy levels of defect complexes based on hybrid functionals exist only for $CuInSe_2$ [24] and not for $CuGaSe_2$. Therefore we leave the A3x unattributed for the time being. However, the Hall studies on epitaxial and polycrystalline $CuGaSe_2$ films [17] indicate that an acceptor with an ionization energy of 120–140 meV exists in $CuGaSe_2$ as well.

At low temperatures all these shallow acceptors are observed in photoluminescence in the form of DA transitions, starting from a shallow donor D1 in $CuInSe_2$ and $CuGaSe_2$. All five theoretical studies find the In_{Cu} antisite as a shallow donor. Those who investigated the Cu_i interstitial find also this defect as a shallow donor. Thus we attribute the D1 defect in $CuInSe_2$ to these two defects. In_{Cu} has lower formation energies in Cu-poor material [127]. This defect is therefore expected to be the dominant donor in the Cu-poor composition range and is responsible for the compensation of defects observed for Cu-poor $CuInSe_2$ [11,20]. The Cu_i interstitial, on the other hand, was calculated with the lowest formation energies in the Cu-rich composition range [127] and is therefore expected to be the dominant donor in material grown under Cu excess. A shallow (artificial) In_{Cu} antisite was found in $CuGaSe_2$ as well [127]. This result implies that both Cu_i and

In_{Cu} act as shallow donors in $CuInSe_2$ and $Cu(In, Ga)Se_2$. In pure $CuGaSe_2$ the In_{Cu} does not exist and the Ga_{Cu} antisite has been predicted as a deep donor, which is discussed in the next section. Therefore in $CuGaSe_2$ the shallow donor D1 is attributed to the Cu_i interstitial alone.

B. Deep defects

A major difference between $CuInSe_2$ and $CuGaSe_2$ is that all theoretical studies on $CuInSe_2$ find the In_{Cu} antisite to be a shallow donor, whereas in $CuGaSe_2$ the Ga_{Cu} antisite is found to be a deep donor with several charge states around 0.4 eV below the conduction band [127,139]. This agrees well with the deep donor DD2 found in the PL of $CuGaSe_2$, which becomes more and more shallow when adding In and merges with the conduction band for Ga/Ga+In ratios below 0.5 (Fig. 6). This defect shows strong phonon coupling with a Huang-Rhys factor of nearly 5 (Fig. 5), indicating that a change in charge state leads to a strong lattice distortion. The III_{Cu} defect has been discussed in the context of a DX center, where the Ga or In shifts to an interstitial site, leaving a Cu vacancy behind [126]. Recent calculations [127] confirm a DX behavior only for the Ga_{Cu} antisite, but this is the defect we are considering here. It is therefore likely that the strong phonon coupling is caused by a shift of the Ga atom away from the Cu site upon charging with one or two electrons. We therefore attribute the DD2 defect to the Ga_{Cu} antisite. The corresponding transition at 1.1 eV has been observed in $CuGaSe_2$ previously [141], albeit much broader, and has been assigned to a DA transition between the Ga_{Cu} and the Cu_{Ga} antisite defects. Since we attribute the A2 acceptor to the Cu_{Ga} antisite, we are in complete agreement with this previous interpretation.

The transition related to the DD1 defect (at around 1.25 eV, see Fig. 4) decreases strongly in intensity as soon as a small amount of In is added. With 20% of In, it is no longer visible. Recent DFT calculations [139] propose this transition to be to a bound-to-free transition from the same Ga_{Cu} defect. However, the peak energy shift with excitation intensity clearly shows that both transitions are donor-acceptor transitions, with the same shallow acceptor involved [80]. Also, this attribution could not explain why this transition disappears with the addition of In. There is only one other DFT calculation on defects in $CuGaSe_2$ [127]. Pohl and Albe propose several charge states of the Ga_{Cu} antisite with slightly different energies in this energy range, which could be the DD1 and DD2 defects that were observed in $CuGaSe_2$. By adding In, another antisite becomes possible—In_{Cu}, which has been calculated as a shallow donor, even in $CuGaSe_2$ [127]. It is conceivable that this additional state near the conduction band edge would change the charge balance between the 0/+1 state and the +1/+2 state in favor of the deeper (the latter) one. Thus we conclude that the DD2 donor is due to the Ga_{Cu} antisite defect and propose the DD1 as the lower charge state of this defect. The DD1 at about 250 meV below the conduction band is then the 0/+1 level and the DD2 the +1/+2 level.

The comparison between energy levels obtained from PL peak energies and those obtained from the theoretical charge transition levels can be quite problematic due to the

Franck-Condon shift (see Fig. 11 in Appendix A), in particular for deep defects where the electron-phonon coupling is strong. However, we would like to stress that all experimental defect energies discussed so far in Secs. V A and V B are based on zero-phonon line energies. Zero-phonon line energies are by definition equal to the energy difference between the equilibrium positions (E_0 in Fig. 11), and this is equal to the transition energies calculated from the crossover points in formation energy vs Fermi-level plots. We argue, therefore, that our comparison between defect energies extracted from zero-phonon lines and those determined from transition points is correct.

Another deep-level DS was found to consist of a broad density of states at around 0.8 eV above the valence band in $CuInSe_2$ and $CuGaSe_2$. If we assume that this level is due to a point defect, the theoretical prediction in Fig. 9 reveals two options that could explain the energy position of this defect in $CuInSe_2$: the third charge state of the V_{In} vacancy or the second charge state of the Cu_{In} antisite. Both explanations would agree with the observation that this transition is more often observed in Cu-rich $Cu(In, Ga)Se_2$. V_{In} has been assigned to the A3 defect, which is observed only in $CuInSe_2$ films grown under high Se supply. However, the DS-related transition is present in films without the DA3 transition as well. Furthermore, the In vacancy has been calculated to have a high formation energy, already making the first charge state improbable under most growth conditions, which is why the third charge state must be even more improbable. We therefore propose the second charge state of the Cu_{In} antisite as the defect of the DS state, in agreement with the proposed attribution in the literature [127]. In $CuGaSe_2$ the Cu_{Ga} antisite is predicted at a very similar energy. In $Cu(In, Ga)Se_2$ the defect should therefore be labeled as the Cu_{III} antisite. It has been observed in Cu-rich and in Cu-poor samples, which is in agreement with neutron scattering data, which found this antisite in both compositional regions [22]. However, by PL we find it mostly in Cu-rich films [Fig. 7(a)], which supports the assignment to a defect that is more likely with higher Cu. However, this attribution cannot explain why the density of states should be broad. An alternative explanation, which might explain the broad density of states, is structural defects, such as grain boundaries or dislocations. Grain boundaries exist obviously only in polycrystalline films. Dislocations have been found with a higher density in epitaxial films [142] than in polycrystalline films [143]. To explain the observed defect transition, which appears very similarly in epitaxial and in polycrystalline films, grain boundaries and dislocations would have to show very similar electronic states. This appears to be very unlikely, taking into account that grain boundaries appear as active recombination centers whereas dislocations do not quench the luminescence [144]. Deep defects have been predicted to form in dislocations around an energy of about 0.5 eV above the valence band [145], which is not in agreement with the defect energy of the DS state. We therefore assign the DS state tentatively to a point defect, namely, the $Cu_{III}^{-1/-2}$ state, keeping in mind that this assignment does not provide a good explanation as to why the density of states should be so broad.

This leaves only the D2 defect unassigned, which was observed in Hall measurements of epitaxial Cu-poor $CuInSe_2$.

We found it to be about 100 meV below the conduction band. The only states around this value in the studies summarized in Fig. 9 are attributed to the V_{Se} vacancy and the In_i interstitial. The In interstitial has a formation energy above 5 eV [24], which excludes this defect. A defect related to the V_{Se} vacancy would agree with the fact that these films were grown by MOVPE with a rather low Se supply. However, the V_{Se} state predicted by theory in Fig. 9 near the conduction band is the 0/-1 transition and not a donor state. Furthermore, the V_{Se} vacancy was found by positron annihilation to exist primarily in the V_{Se}-V_{Cu} vacancy complex in Cu-poor $CuInSe_2$ epitaxial films [120]. This double vacancy has been predicted to present a shallow donor state [146]. This donor state was confirmed by recent GW calculations [147]. The defects related to the V_{Se} vacancy are metastable, however [79,148]. The Hall measurements were performed on *n*-type material with a rather high carrier concentration. In this case the V_{Se}-V_{Cu} double vacancy could be rather in its acceptor state [146]. If we, however, assume that the observed donor is caused by those double vacancies that remain in the donor state, the metastable behavior of the double vacancy could also explain why we never see the D2 donor in PL measurements: upon illumination, the double vacancy captures electrons and changes from a donorlike state to an acceptorlike state. Thus the donorlike state of the double vacancy is not observable under illumination, i.e., in PL. Therefore we attribute the D2 donor tentatively to the donor state of the V_{Se}-V_{Cu} double vacancy.

In summary, using the recent defect calculations based on hybrid and on GW functionals we could assign all experimentally observed defects, at least tentatively, to a specific point defect. The assignments are summarized in Table I. We would like to point out that we are very confident with the assignments of A1, A2, D1, and DD2—and less so with the other assignments, as discussed earlier in this section.

VI. CONSEQUENCES FOR SOLAR CELLS

$Cu(In, Ga)Se_2$ solar cells are based on *p*-type absorbers. Devices are typically grown on soda-lime glass, which supplies sodium into the film by diffusion from the substrate. It has been known for a long time that Na increases the *p*-type doping in $Cu(In, Ga)Se_2$ [149]. However, there is no evidence that Na introduces additional electronic states, which is confirmed by the similarity of the PL spectra between epitaxial and polycrystalline films, discussed in this contribution. A theoretical study of the effect of various alkalis on $CuInSe_2$ indicates that none of the alkalis introduces extra defect states in the gap [9]. A recent review and discussion of the doping mechanisms of Na can be found in Ref. [150], where the Na incorporation at higher temperatures during growth or postdeposition treatment led to Na_{Cu} defects. But at lower temperatures the Na diffuses out and leaves Cu vacancies behind. Other explanations invoke a removal of compensating In_{Cu} antisites [151]. Thus, we can conclude that the *p*-type doping originates from native defects. This doping is caused by the two acceptors found in PL in Cu-rich $CuInSe_2$ and $CuGaSe_2$: the Cu vacancy V_{Cu} and the Cu_{III} antisite. Both defects have been confirmed by neutron scattering in Cu-poor material as well [22]. These acceptors are partly compensated by one, possibly two donors: the Cu interstitial and the In_{Cu}
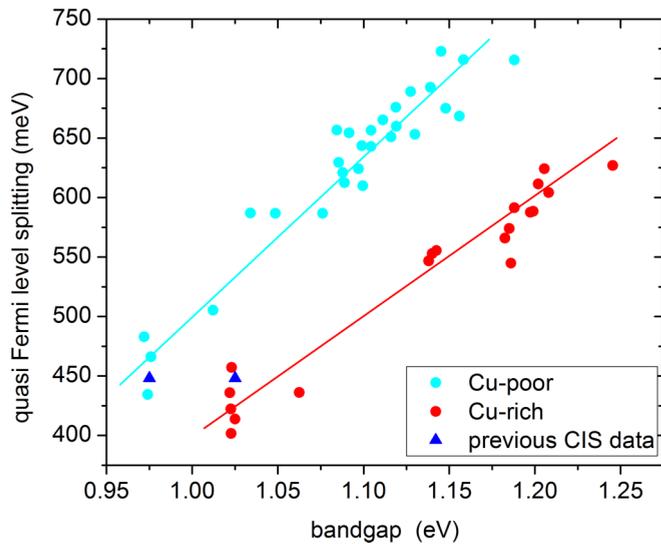
FIG. 10. Quasi-Fermi-level splitting of Cu-rich and Cu-poor Cu(In, Ga)Se$_2$. Higher Ga content leads to a higher band gap. The lines are a guide to the eye. It is seen that Cu-poor material has always a higher quasi-Fermi-level splitting, i.e., less nonradiative recombination. The triangles indicate the result of a previous investigation of pure CuInSe$_2$ [156]. The difference between Cu-rich and Cu-poor material increases with increasing Ga content. This behavior is attributed to the fact that the DS state becomes deeper and thus more recombination active with increasing Ga content.

FIG. 11. Energy schematics of a PL transition involving a defect with a Franck-Condon shift.

antisite. The compensation is stronger in Cu-poor material than in Cu-rich material (see the discussion of Fig. 1 and Refs. [19] and [20]).

Deep defects are very critical for the performance of a solar cell, since they provide recombination centers which decrease the quasi-Fermi-level splitting and thus the open-circuit voltage. According to the experimental and theoretical results reviewed here, two defects form deep states: The Ga$_{Cu}$ antisite (DD2) forms a deep donor. Another deep defect DS could be related to the second charge state of the Cu$_{III}$ antisite. The DD2 defect (Ga$_{Cu}$ antisite) becomes shallower and thus less critical for recombination [152] when adding In to CuGaSe$_2$ and finally merges with the conduction band below a Ga/Ga+In ratio of 0.5 (Fig. 6). DD2 is thus an effective recombination center only for Cu(In, Ga)Se$_2$ with high Ga content. It has been known that the open-circuit voltage loss in Cu(In, Ga)Se$_2$ solar cells increases for high Ga contents, particularly for Ga ratios higher than 0.3 [87]. While a range of effects will play a role in this increased loss behavior, the turning of the DD2 into a recombination center will certainly play an important role.

The DS state is more obvious in Cu-rich than in Cu-poor materials [Fig. 7(a)]. It could thus be at least partly responsible for the lower performance of Cu-rich Cu(In, Ga)Se$_2$ solar cells. It is well known that Cu-rich Cu(In, Ga)Se$_2$ solar cells suffer from recombination at or near the interface [153], which can be attributed to the formation of a defect near the surface due to the necessary etching process [154]. However, it was recently shown that also the bulk of Cu-rich Cu(In, Ga)Se$_2$ suffers from a higher degree of recombination, as evidenced by a lower quasi-Fermi-level splitting in Cu-rich absorbers
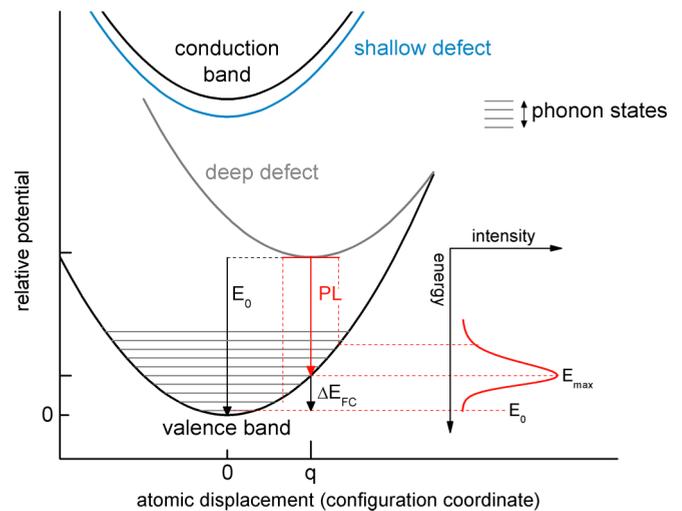
than in Cu-poor ones [155]. An update of this observation over a wider range of compositions and band gaps is shown in Fig. 10. In a previous investigation, we had found almost the same quasi-Fermi-level splitting in Cu-rich and Cu-poor CuInSe$_2$ [156]. However, in that study we did not take into account the lower band gap of Cu-poor material compared to Cu-rich material [157]. Those previous measurements of pure CuInSe$_2$ are shown as triangles in Fig. 10 and confirm the trend of lower quasi-Fermi-level splitting in Cu-rich material, when we take the difference in band gap into account. What becomes obvious from Fig. 10 is that the difference between the quasi-Fermi-level splitting in Cu-poor and Cu-rich Cu(InGa)Se$_2$ increases with increasing band gap, i.e., with increasing Ga content. This behavior can be explained by the properties of the DS state: it is more present in Cu-rich Cu(In, Ga)Se$_2$ than in Cu-poor material, and it becomes deeper and more recombination active with increasing Ga content. Thus, while the DS center already acts as a recombination center in Cu-rich CuInSe$_2$, it becomes deeper with increasing Ga content and consequently increases the difference between Cu-rich and Cu-poor Cu(In, Ga)Se$_2$.

Concerning the deep states, we can thus say that the DD2 defect, attributed to the Ga$_{Cu}$ antisite, explains, at least partly, the problematic behavior of *high-Ga* Cu(In, Ga)Se$_2$ absorbers. And the DS, possibly due to the second charge state of the Cu$_{III}$ antisite, explains the higher recombination in the bulk of *Cu-rich* Cu(In, Ga)Se$_2$. It should be noted that in high-efficiency Cu(In, Ga)Se$_2$ absorbers, which results in solar cells with 20% efficiency and above, no deep defects are observed by PL, even without any heavy alkali postdeposition treatment [96]. Thus, both the DD2 and the DS defect have to be avoided to obtain high-efficiency solar cells.

VII. CONCLUSIONS

We present new results on deep defects in Cu(In, Ga)Se$_2$ studied by photoluminescence and combine them with results from the literature and obtained by other experimental methods. We compare the observed defect energies to the

FWHM: 2 meV

FWHM: 50 meV
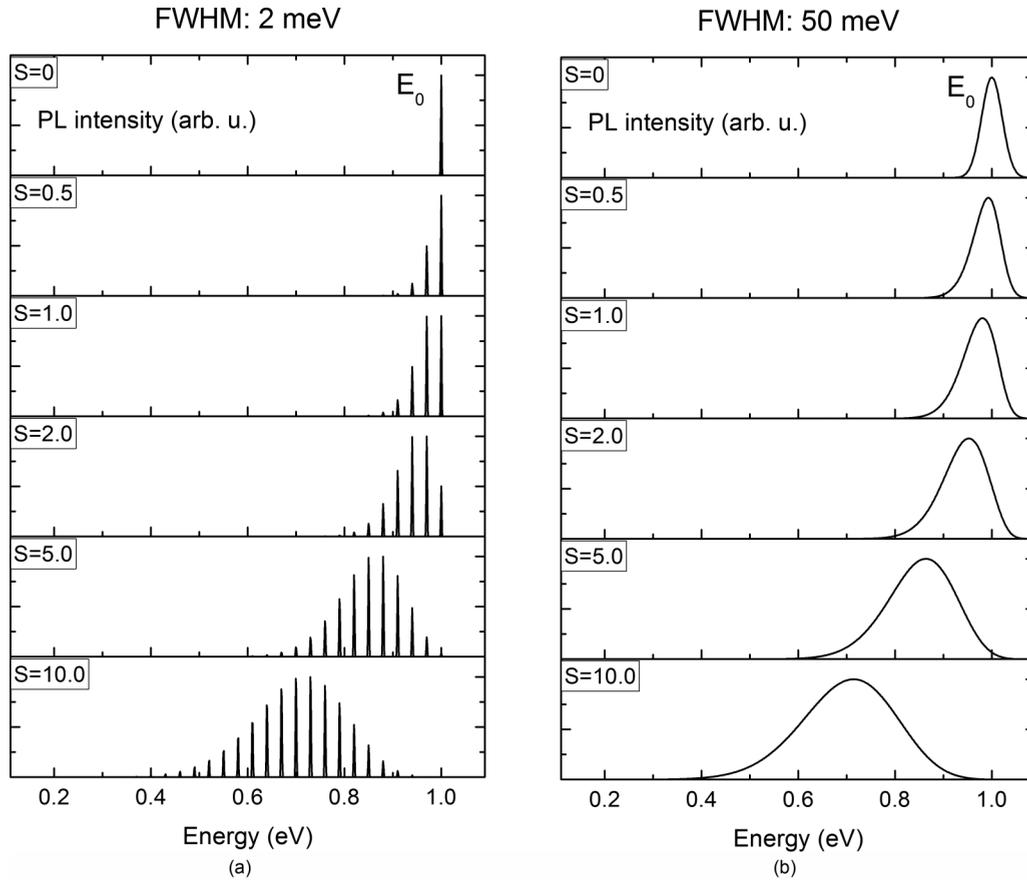
FIG. 12. (a) Equation (A1) with negligible Gaussian broadening and with increasing Huang-Rhys factor S, and (b) the same but with a Gaussian broadening of 50 meV.

results of a number of recent calculations based on hybrid and GW functionals. The experimental results are summarized in Fig. 8, and the assignments with the help of the calculated defects are given in Table I. We confirm two shallow acceptors in CuInSe$_2$ and CuGaSe$_2$: the V_{Cu} vacancy and the Cu$_{III}$ antisite. Furthermore, in CuInSe$_2$ and low-Ga Cu(In, Ga)Se$_2$, grown with a high Se supply, we identify a third acceptor, likely the V_{In} vacancy. These acceptors are compensated by one, possibly two shallow donors: the In$_{Cu}$ antisite and the Cu$_i$ interstitial, plus a further deeper donor, which is possibly due to the V_{Se}-V_{Cu} double vacancy. Two different deep defects are critical for solar cell performance: the Ga$_{Cu}$ antisite forms a deep donor in high-Ga Cu(In, Ga)Se$_2$ and plays a role in the stronger open-circuit voltage loss of these wider-band-gap solar cells. A deep defect at about 0.8 eV above the valence is more prominent in Cu-rich material. This recombination center limits the open-circuit voltage of Cu-rich solar cells, more so with higher Ga/Ga+In ratio. While the intrinsic shallow point defects control the doping and are thus essential for the solar cells, the deep defects are detrimental for the performance of Cu(In, Ga)Se$_2$-based solar cells and have to be avoided.

ACKNOWLEDGMENTS

APPENDIX A: PHONON COUPLING OF DEEP DEFECTS

Charge changes in deep defects very often lead to a lattice relaxation, leading to a Franck-Condon shift. The emission from such a defect can be described by a model first proposed by Huang and Rhys [158]. The equilibrium lattice configuration around such a defect is different for the different charge states. Thus, upon an electronic transition the lattice will relax to the new equilibrium configuration, involving the movement of atoms, which invokes the emission of phonons. The atomic positions are generally summarized in the configuration coordinate, and the energetics are described in a configuration diagram as in Fig. 11. A tutorial description can be found, for example, in Ref. [61].

The spectral shape is determined by a Poisson distribution of Gaussian transitions, shifted by the phonon energy:

$$I(\hbar\omega) \sim \sum_n \exp(-S)\frac{S^n}{n!}\exp\left[-\frac{1}{2}\left(\frac{E_0 - n\hbar\Omega - \hbar\omega}{\sigma}\right)^2\right],$$

(A1)

where I is the intensity at a photon energy of $\hbar\omega$, S is the Huang-Rhys factor, which equals the ratio of the phonon energy $\hbar\Omega$ to the Franck-Condon shift ΔE_{FC}, E_0 the zero-phonon line, and σ a Gaussian broadening of the transitions. For an explanation of the different quantities see Fig. 11. It should be noted that in experiments that rely on thermal activation and determine an activation energy, such as Hall measurements or admittance spectroscopy, the energy difference between the equilibrium positions is measured, i.e., the zero phonon energy E_0.

To better understand the influence of the different parameters, we show in Fig. 12 a plot of the intensity according to Eq. (A1). The left panel shows the effect of an increasing Franck-Condon shift. The phonon energy is kept constant at 30 meV, and thus an increasing Franck-Condon shift corresponds to an increasing Huang-Rhys factor S. With $S = 0$ (no shift), we see only the zero-phonon line, which is assumed at 1 eV. With a small S, we see the zero-phonon line plus phonon replicas with decreasing intensity. When S becomes >1, the maximum or the emission spectrum shifts away from the zero-phonon line, more so with higher S. With a Gaussian broadening (right panel in Fig. 12) we see the peak shape obtained experimentally; see. Fig. 3 of the paper.

APPENDIX B: CROSS-CORRELATION COEFFICIENT

The calculation of the cross-correlation coefficient $C_C(A, B)$ between two maps A and B is

$$C_C(A, B) = \frac{1}{n} \sum_{i,j} \frac{[A(i,j) - \overline{A(i,j)}][B(i,j) - \overline{B(i,j)}]}{\sigma[A(i,j)]\sigma[B(i,j)]}$$

(B1)

with n the number of pixels in each map, $\overline{A(i,j)}$ the mean value of the map A, and $\sigma[A(i,j)]$ the standard deviation of map A. The cross-correlation coefficient can vary between -1 (totally anticorrelated) to 1 (totally correlated).

APPENDIX C: Ga/Ga+In DEPENDENCE OF THE DD2 DEFECT LUMINESCENCE IN Cu-Poor Cu(In, Ga)Se$_2$

Figure 13 shows the PL of a series of Cu-poor epitaxial Cu(In,Ga)Se$_2$ films, indicating again the deep defect transition at 1.1 eV.

APPENDIX D: THE 0.8-eV DEFECT IN PL

Figure 14 shows a number of PL measurements on various epitaxial and polycrystalline Cu(In,Ga)Se$_2$ samples, indicating that the peak 0.7 or 0.8 eV is rather ubiquitous, but considerably weaker in Cu-poor samples.

APPENDIX E: COMPARISON BETWEEN PL MEASUREMENTS AND DEFECTS FROM CAPACITANCE AND TRANSPORT MEASUREMENTS

Here we discuss defects that have been observed in electrical measurements but not in PL measurements. We refer to the labels in Ref. [93].
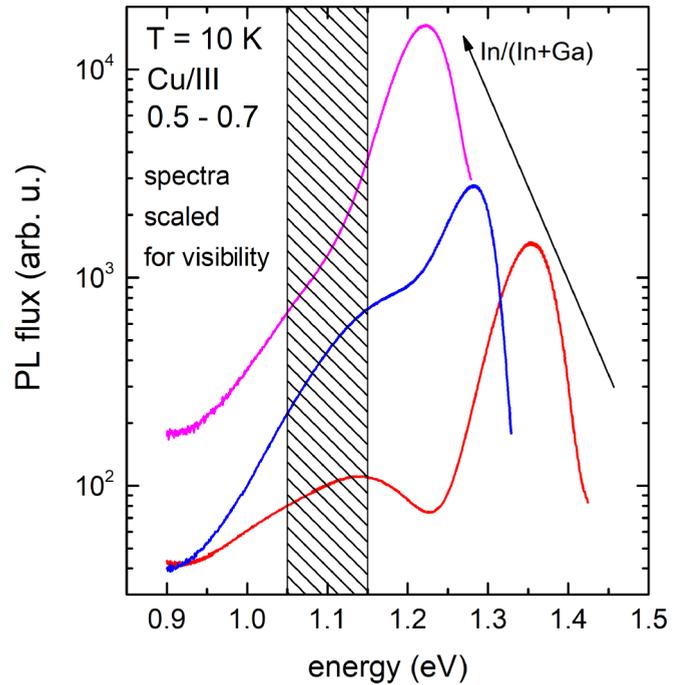
FIG. 13. PL spectra measured at 10 K for a set of Cu-poor Cu(In, Ga)Se$_2$ epitaxial films on GaAs with varying In/In+Ga ratio. The highest energy peak in all spectra is the near-band-edge transition, which shifts to lower energies with higher In/In+Ga ratio. All films show a deep transition (DD2-A2) at around 1.1 eV (hashed area) that shifts only very little with varying composition and indicates a deep defect at an energy independent of the In/In+Ga ratio.

A defect we cannot relate to our PL (or Hall) measurements is the E1 defect in CuInSe$_2$. In CuGaSe$_2$ the E1 is in the energy range of the DD2 deep donor, but as we discuss above, DD2 merges into the conduction band below a Ga/Ga+In ratio of about 0.5. E3 is mentioned in Refs. [93] and [159] as being likely the same as E1. E4 and PC1 have also no equivalent in the PL/Hall measurements. They are particular defects, as their emission rate is strongly dependent on the hole concentration. This has been attributed [93,126] to a metastable behavior similar to a DX defect. It is conceivable that this is why they are not detected in PL with its rather strong illumination. The E4 is generally identified with the N2 defect [107] as well as with defects labeled A2 and A4 in CuGaSe$_2$ [159,160]. It has been shown to exhibit metastable behavior, which could explain why we do not detect it in PL. We also do not detect E5, which appeared only in the most Cu-poor sample. It is possible that this defect occurs in a Cu-poor phase such as CuGa$_3$Se$_5$ [161] or CuGa$_5$Se$_8$ [162], which have wider band gaps and likely a lower valence-band maximum [163]. Another defect which we do not observe in PL and Hall measurements is the PC2, which was found to show metastable behavior by a time dependence of the observed density of states at elevated temperatures [164], which could explain why we do not see it in PL measurements. Furthermore, since its density of states increases with time at
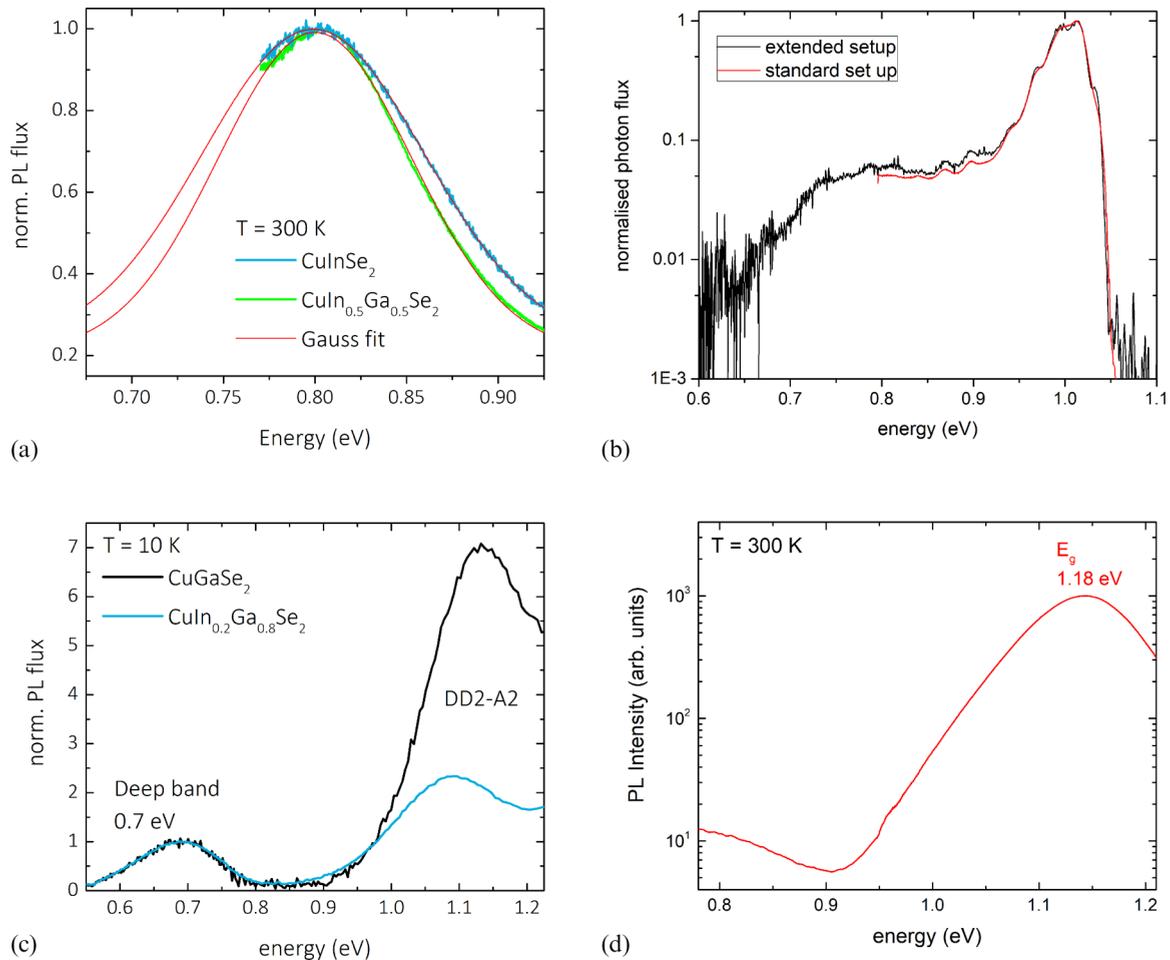
FIG. 14. PL spectra showing the transition at around 0.7 or 0.8 eV. (a) Room temperature PL of an epitaxial $CuInSe_2$ and an epitaxial $Cu(In,Ga)Se_2$ sample with Ga/Ga+In ratio of 0.5, both are Cu-rich. (b) Low temperature PL of a polycrystalline Cu-rich $CuInSe_2$ film, indicating that the deep luminescence peak can only be distinguished from a background signal with the extended set-up, measureing at low enough energies. (c) Low temperature PL of an epitaxial $CuGaSe_2$ and an epitaxial $Cu(In,Ga)Se_2$ sample with Ga/Ga+In ratio of 0.8, both are Cu-rich. It should be noted that the room temperature spectra of high Ga $Cu(In,Ga)Se_2$ are dominated by the broad DD2 transition, which covers any weaker transition in the energy region around 0.8 eV. (d) Room temperature PL of a slightly Cu-poor epitaxial $Cu(In,Ga)Se_2$ sample with Ga/Ga+In of 0.3. Note the log-scale. The 0.8 eV defect luminescence is very weak.

elevated temperature and since it is only observed in samples on glass, one might suspect that it is related to oxidation or diffusion of elements from the glass and it might not be a native defect.

[1] A. Chirila *et al.*, Nat. Mater. **12**, 1107 (2013).

[2] Solar Frontier Achieves: World Record Thin-Film Solar Cell Efficiency of 23.35%, http://www.solar-frontier.com/eng/news/2019/0117_press.html (accessed January 2019).

[3] P. Jackson, R. Wuerz, D. Hariskos, E. Lotter, W. Witte, and M. Powalla, Phys. Status Solidi RRL **10**, 583 (2016).

[4] T. Kato, Jpn. J. Appl. Phys. **56**, 04CA02 (2017).

[5] H. Elanzeery, F. Babbe, M. Melchiorre, F. Werner, and S. Siebentritt, Prog. Photovoltaics Res. Appl. **26**, 437 (2018).

[6] T. Feurer, B. Bissig, T. P. Weiss, R. Carron, E. Avancini, J. Löckinger, S. Buecheler, and A. N. Tiwari, Sci. Technol. Adv. Mater. **19**, 263 (2018).

[7] F. Larsson, N. S. Nilsson, J. Keller, C. Frisk, V. Kosyak, M. Edoff, and T. Torndahl, Prog. Photovoltaics Res. Appl. **25**, 755 (2017).

[8] S. Siebentritt, Nat. Energy **2**, 840 (2017).

[9] M. Malitckaya, H. P. Komsa, V. Havu, and M. J. Puska, J. Phys. Chem. C **121**, 15516 (2017).

[10] S. Zott, K. Leo, M. Ruckh, and H. W. Schock, Appl. Phys. Lett. **68**, 1144 (1996).

[11] I. Dirnstorfer, M. Wagner, D. M. Hofmann, M. D. Lampert, F. Karg, and B. K. Meyer, Phys. Status Solidi A **168**, 163 (1998).

[12] T. Gödecke, T. Haalboom, and F. Ernst, Z. Metallkd. **91**, 622 (2000).

[13] M. Fearheiley, Solar Cells **16**, 91 (1986).

[14] J. C. Mikkelsen, Jr., J. Electron. Mater. **10**, 541 (1981).

[15] S. Siebentritt, L. Gütay, D. Regesch, Y. Aida, and V. Deprédurand, Solar Energy Mater. Solar Cells **119**, 18 (2013).

[16] N. Rega, S. Siebentritt, J. Albert, S. Nishiwaki, A. Zajogin, M. C. Lux-Steiner, R. Kniese, and M. J. Romero, Thin Solid Films **480–481**, 286 (2005).

[17] S. Schuler, S. Siebentritt, S. Nishiwaki, N. Rega, J. Beckmann, S. Brehme, and M. C. Lux-Steiner, Phys. Rev. B **69**, 045210 (2004).

[18] M. Wagner, I. Dirnstorfer, D. M. Hofmann, M. D. Lampert, F. Karg, and B. K. Meyer, Phys. Status Solidi A **167**, 131 (1998).

[19] A. Bauknecht, S. Siebentritt, J. Albert, and M. C. Lux-Steiner, J. Appl. Phys. **89**, 4391 (2001).

[20] S. Siebentritt, N. Rega, A. Zajogin, and M. C. Lux-Steiner, in *Conference on Photo-Responsive Materials*, edited by A. W. R. Leitch and R. Botha (Wiley, Kariega Game Reserve, South Africa, 2004), p. 2304.

[21] J. Larsen, K. Burger, L. Gütay, and S. Siebentritt, in *37th IEEE Photovoltaic Specialist Conference* (IEEE, Seattle, 2011), p. 396.

[22] C. Stephan, S. Schorr, M. Tovar, and H.-W. Schock, Appl. Phys. Lett. **98**, 091906 (2011).

[23] S. B. Zhang, S.-H. Wei, and A. Zunger, Phys. Rev. Lett. **78**, 4059 (1997).

[24] M. Malitckaya, H.-P. Komsa, V. Havu, and M. J. Puska, Adv. Electron. Mater. **3**, 1600353 (2017).

[25] B. I. Shklovskii and A. L. Efros, *Electronic Properties of Doped Semiconductors* (Springer-Verlag, Berlin, 1984).

[26] P. W. Yu, J. Appl. Phys. **47**, 677 (1976).

[27] S. Siebentritt, N. Papathanasiou, and M. C. Lux-Steiner, Physica B **376–377**, 831 (2006).

[28] S. Siebentritt, in *Wide Gap Chalcopyrites*, edited by S. Siebentritt and U. Rau (Springer, Berlin, 2006), p. 113.

[29] P. Migliorato, J. L. Shay, H. M. Kasper, and S. Wagner, J. Appl. Phys. **46**, 1777 (1975).

[30] P. W. Yu, Solid State Commun. **18**, 395 (1976).

[31] G. Massé, J. Phys. Chem. Solids **45**, 1091 (1984).

[32] F. A. Abou-Elfotouh, D. J. Dunlavy, D. Cahen, R. Noufi, L. L. Kazmerski, and K. J. Bachmann, Prog. Cryst. Growth Charact. **10**, 365 (1985).

[33] S. Niki, Y. Makita, A. Yamada, A. Obara, S. Misawa, O. Igarashi, K. Aoki, and N. Kutsuwada, Jpn. J. Appl. Phys. **33**, L500 (1994).

[34] S. Niki, Y. Makita, A. Yamada, and A. Obara, Sol. Energy Mater. Sol. Cells **35**, 141 (1994).

[35] S. Niki, H. Shibata, P. J. Fons, A. Yamada, A. Obara, Y. Makita, T. Kurafuji, S. Chichibu, and H. Nakanishi, Appl. Phys. Lett. **67**, 1289 (1995).

[36] M. A. Abdullaev, Soviet Physics - Semicond. **26**, 1196 (1992).

[37] S. Zott, K. Leo, M. Ruckh, and H. W. Schock, J. Appl. Phys. **82**, 356 (1997).

[38] A. V. Mudryi, I. V. Bodnar, V. F. Gremenok, I. A. Victorov, A. I. Patuk, and I. A. Shakin, Sol. Energy Mater. Sol. Cells **53**, 247 (1998).

[39] A. V. Mudryi, I. V. Bodnar, I. A. Victorov, V. F. Gremenok, M. V. Yakushev, R. D. Tomlinson, A. E. Hill, and R. D. Pilkington, Appl. Phys. Lett. **77**, 2542 (2000).

[40] M. V. Yakushev, F. Luckert, C. Faugeras, A. V. Karotki, A. V. Mudryi, and R. W. Martin, Appl. Phys. Lett. **97**, 152110 (2010).

[41] D. S. Nedzvetskii, I. V. Bodnar, V. A. Gaisin, and A. Y. Serov, Opt. Spectrosc. **52**, 340 (1982).

[42] S. Shirakata, K. Tamura, and S. Isomura, Jpn. J. Appl. Phys. **35**, L531 (1996).

[43] A. Yamada, Y. Makita, S. Niki, A. Obara, P. Fons, H. Shibata, M. Kawai, S. Chichibu, and H. Nakanishi, J. Appl. Phys. **79**, 4318 (1996).

[44] S. Chichibu, H. Nakanishi, S. Shirakata, S. Isomura, H. Miyake, and K. Sugiyama, Appl. Phys. Lett. **71**, 533 (1997).

[45] K. Tanaka, H. Uchiki, and S. Iida, Jpn. J. Appl. Phys. **38**, 1329 (1999).

[46] F. Luckert, M. V. Yakushev, C. Faugeras, A. V. Karotki, A. V. Mudryi, and R. W. Martin, Appl. Phys. Lett. **97**, 162101 (2010).

[47] G. Massé and E. Redjai, J. Phys. Chem. Solids **47**, 99 (1986).

[48] G. Massé, N. Lahlou, and N. Yamamoto, J. Appl. Phys. **51**, 4981 (1980).

[49] K. Yoshino, M. Sugiyama, D. Maruoka, S. Chichibu, H. Komaki, K. Umeda, and T. Ikari, Physica B **302–303**, 357 (2001).

[50] H. Weinert, H. Neumann, H.-J. Höbler, G. Kühn, and N. van Nam, Phys. Status Solidi B **81**, K59 (1977).

[51] E. Arushanov, L. Essaleh, J. Galibert, J. Leotin, and S. Askenazy, Physica B **184**, 229 (1993).

[52] H. Neumann, H. Sobotta, W. Kissinger, V. Riede, and G. Kühn, Phys. Status Solidi B **108**, 483 (1981).

[53] K. K. Chattopadhyay, I. Sanyal, S. Chaudhuri, and A. K. Pal, Vacuum **42**, 915 (1991).

[54] C. Persson, Appl. Phys. Lett. **93**, 072106 (2008).

[55] P. Yu and M. Cardona, *Fundamentals of Semiconductors* (Springer-Verlag, Berlin Heidelberg, 2010), p. 398.

[56] W. N. Shafarman, S. Siebentritt, and L. Stolt, in *Handbook of Photovoltaic Science and Engineering,* 2nd ed., edited by A. Luque and S. Hegedus (Wiley and Sons, Chichester, UK, 2010), p. 546.

[57] I. V. Bodnar, A. G. Karoza, and G. F. Smirnova, Phys. Status Solidi B **84**, K65 (1977).

[58] F. J. Ramirez and C. Rincón, Solid State Commun. **84**, 551 (1992).

[59] N. N. Syrbu, M. Bogdanash, V. E. Tezlevan, and I. Mushcutariu, Physica B **229**, 199 (1997).

[60] H. Tanino, T. Maeda, H. Fujikake, H. Y. Nakanishi, S. Endo, and T. Irie, Phys. Rev. B **45**, 13323 (1992).

[61] A. Alkauskas, M. D. McCluskey, and C. G. Van de Walle, J. Appl. Phys. **119**, 181101 (2016).

[62] P. R. C. Kent and A. Zunger, Phys. Rev. Lett. **86**, 2613 (2001).

[63] W. Shan, W. Walukiewicz, J. W. M. Yu, J. W. Ager, S. Siebentritt, and N. Rega, Phys. Status Solidi B **241**, 3117 (2004).

[64] K. Hönes, M. Eickenberg, S. Siebentritt, and C. Persson, Appl. Phys. Lett. **93**, 092102 (2008).

[65] S. Siebentritt, S. Augustin, N. Papathanasiou, D. Hebert, A. Rockett, J. Bläsing, and M. C. Lux-Steiner, Mater. Res. Soc. Symp. Proc. **1012**, 483 (2007).

[66] S. Siebentritt, M. Igalson, C. Persson, and S. Lany, Prog. Photovoltaics Res. Appl. **18**, 390 (2010).

[67] F. Babbe, H. Elanzeery, M. H. Wolter, K. Santosh, and S. Siebentritt, J. Phys.: Condens. Matter **31**, 425702 (2019).

[68] S. Siebentritt, Thin Solid Films **403–404**, 1 (2002).

[69] S. Siebentritt, I. Beckers, T. Riemann, J. Christen, A. Hoffmann, and M. Dworzak, Appl. Phys. Lett. **86**, 091909 (2005).

[70] J. Larsen, Ph.D. thesis, University of Luxembourg, 2011, http://orbilu.uni.lu/handle/10993/15580.

[71] G. Massé and E. Redjai, J. Appl. Phys. **56**, 1154 (1984).

[72] M. V. Yakushev, Y. Feofanov, R. W. Martin, R. D. Tomlinson, and A. V. Mudryi, J. Phys. Chem. Solids **64**, 2011 (2003).

[73] S. Chatraphorn, K. Yoodee, P. Songpongs, C. Chityuttakan, K. Sayavong, S. Wongmanerod, and P. O. Holtz, Jpn. J. Appl. Phys. **37**, L269 (1998).

[74] R. Noufi, R. Axton, C. Herrington, and S. K. Deb, Appl. Phys. Lett. **45**, 668 (1984).

[75] F. Werner, D. Colombara, M. Melchiorre, N. Valle, B. E. Adib, C. Spindler, and S. Siebentritt, J. Appl. Phys. **119**, 173103 (2016).

[76] H. Neumann, R. D. Tomlinson, N. Avgerinos, and E. Nowak, Phys. Status Solidi A **75**, K199 (1983).

[77] S. M. Wasim, Solar Cells **16**, 289 (1986).

[78] G. Kühn and H. Neumann, Z. für Chemie **27**, 197 (1987).

[79] S. Lany and A. Zunger, Phys. Rev. Lett. **93**, 156404 (2004).

[80] C. Spindler, D. Regesch, and S. Siebentritt, Appl. Phys. Lett. **109**, 032105 (2016).

[81] E. Zacks and A. Halperin, Phys. Rev. B **6**, 3072 (1972).

[82] J. I. Pankove, *Optical Processes in Semiconductors* (Dover Publications, New York, 1975).

[83] M. A. Reshchikov and H. Morkoc, J. Appl. Phys. **97**, 061301 (2005).

[84] A. Alkauskas, J. L. Lyons, D. Steiauf, and C. G. Van de Walle, Phys. Rev. Lett. **109**, 267401 (2012).

[85] A. Klein, J. Phys.: Condens. Matter **27**, 134201 (2015).

[86] R. Scheer, Jpn. J. Appl. Phys. **39**, 371 (2000).

[87] R. Herberholz, V. Nadenau, U. Rühle, C. Köble, H. W. Schock, and B. Dimmler, Sol. Energy Mater. Sol. Cells **49**, 227 (1997).

[88] J. T. Heath, J. D. Cohen, W. N. Shafarman, D. X. Liao, and A. A. Rockett, Appl. Phys. Lett. **80**, 4540 (2002).

[89] S. Niki, R. Suzuki, S. Ishibashi, T. Ohdaira, P. Fons, A. Yamada, H. Oyanagi, T. Wada, R. Kimura, and T. Nakada, Thin Solid Films **387**, 129 (2001).

[90] L. M. Mansfield, D. Kuciauskas, P. Dippo, J. V. Li, K. Bowers, B. To, C. DeHart, and K. Ramanathan, IEEE J. Photovolt. **5**, 1769 (2015).

[91] M. A. Reshchikov, D. O. Demchenko, J. D. McNamara, S. Fernández-Garrido, and R. Calarco, Phys. Rev. B **90**, 035207 (2014).

[92] M. A. Reshchikov and R. Y. Korotkov, Phys. Rev. B **64**, 115205 (2001).

[93] A. Krysztopa, M. Igalson, J. K. Larsen, Y. Aida, L. Gütay, and S. Siebentritt, J. Phys. D: Appl. Phys. **45**, 335101 (2012).

[94] J. Lauwaert, L. Van Puyvelde, J. W. Thybaut, S. Khelifi, M. Burgelman, F. Pianezzi, A. N. Tiwari, and H. Vrielinck, Sol. Energy Mater. Sol. Cells **112**, 78 (2013).

[95] T. Eisenbarth, T. Unold, R. Caballero, C. A. Kaufmann, and H.-W. Schock, J. Appl. Phys. **107**, 034509 (2010).

[96] F. Werner, M. H. Wolter, S. Siebentritt, G. Sozzi, S. Di Napoli, R. Menozzi, P. Jackson, W. Witte, R. Carron, E. Avancini, Th. Weiss, and S. Buecheler, Prog. Photovolt. Res. Appl. **26**, 911 (2018).

[97] F. Werner and S. Siebentritt, Phys. Rev. Appl. **9**, 054047 (2018).

[98] R. Herberholz, M. Igalson, and H. W. Schock, J. Appl. Phys. **83**, 318 (1998).

[99] U. Reislöhner, H. Metzner, and C. Ronning, Phys. Rev. Lett. **104**, 226403 (2010).

[100] J. Luckas, C. Longeaud, and S. Siebentritt, J. Appl. Phys. **116**, 103710 (2014).

[101] W. Meyer and H. Neldel, Z. Tech. Phys. **18**, 588 (1937).

[102] A. Yelon, B. Movaghar, and R. S. Crandall, Rep. Prog. Phys. **69**, 1145 (2006).

[103] R. Widenhorn, A. Rest, and E. Bodegom, J. Appl. Phys. **91**, 6524 (2002).

[104] R. Widenhorn, M. Fitzgibbons, and E. Bodegom, J. Appl. Phys. **96**, 7379 (2004).

[105] R. Baier, J. Lehmann, S. Lehmann, T. Rissom, C. A. Kaufmann, A. Schwarzmann, Y. Rosenwaks, M. C. Lux-Steiner, and S. Sadewasser, Sol. Energy Mater. Sol. Cells **103**, 86 (2012).

[106] J. T. Heath, J. D. Cohen, and W. N. Shafarman, J. Appl. Phys. **95**, 1000 (2004).

[107] A. Krysztopa, M. Igalson, L. Gütay, J. K. Larsen, and Y. Aida, Thin Solid Films **535**, 366 (2013).

[108] A. Urbaniak, K. Macielak, M. Igalson, P. Szaniawski, and M. Edoff, J. Phys.: Condens. Matter **28**, 215801 (2016).

[109] K. Macielak, M. Igalson, P. Zabierowski, N. Barreau, and L. Arzel, Thin Solid Films **582**, 383 (2015).

[110] G. D. Watkins, Phys. Solid State **41**, 746 (1999).

[111] J. Isoya, T. Umeda, N. Mizuochi, N. T. Son, E. Janzen, and T. Ohshima, Phys. Status Solidi B **245**, 1298 (2008).

[112] H. J. v. Bardeleben, A. Goltzene, and C. Schwab, Phys. Status Solidi B **76**, 363 (1976).

[113] T. Nishi, Y. Katsumata, K. Sato, and H. Miyake, Sol. Energy Mater. Sol. Cells **67**, 273 (2001).

[114] M. Birkholz, P. Kanschat, T. Weiss, M. Czerwensky, and K. Lips, Phys. Rev. B **59**, 12268 (1999).

[115] R. Wurz, A. Meeder, D. Fuertes Marron, T. Schedel-Niedrig, A. Knop-Gericke, and K. Lips, Phys. Rev. B **70**, 205321 (2004).

[116] V. Aubin, L. Binet, and J. F. Guillemoles, Thin Solid Films **431–432**, 167 (2003).

[117] V. Aubin, L. Binet, P. Stallworth, and J. F. Guillemoles, J. Phys. Chem. Solids **64**, 1633 (2003).

[118] A. Polity, R. Krause-Rehberg, T. E. M. Staab, M. J. Puska, J. Klais, H. J. Möller, and B. K. Meyer, J. Appl. Phys. **83**, 71 (1998).

[119] F. Börner, J. Gebauer, S. Eichler, R. Krause-Rehberg, I. Dirnstorfer, B. K. Meyer, and F. Karg, Physica B **273–274**, 930 (1999).

[120] E. Korhonen, K. Kuitunen, F. Tuomisto, A. Urbaniak, M. Igalson, J. Larsen, L. Guetay, S. Siebentritt, and Y. Tomm, Phys. Rev. B **86**, 064102 (2012).

[121] L. J. Zhang, T. Wang, J. Li, Y. P. Hao, J. D. Liu, P. Zhang, B. Cheng, Z. W. Zhang, B. Y. Wang, and B. J. Ye, Thin Solid Films **525**, 68 (2012).

[122] M. M. Islam, A. Uedono, S. Ishibashi, K. Tenjinbayashi, T. Sakurai, A. Yamada, S. Ishizuka, K. Matsubara, S. Niki, and K. Akimoto, Appl. Phys. Lett. **98**, 112105 (2011).

[123] A. Uedono, M. M. Islam, T. Sakurai, C. Hugenschmidt, W. Egger, R. Scheer, R. Krause-Rehberg, and K. Akimoto, Thin Solid Films **603**, 418 (2016).

[124] M. M. Islam, A. Uedono, T. Sakurai, A. Yamada, S. Ishizuka, K. Matsubara, S. Niki, and K. Akimoto, J. Appl. Phys. **113**, 064907 (2013).

[125] C. Stephan, T. Scherb, C. A. Kaufmann, S. Schorr, and H. W. Schock, Appl. Phys. Lett. **101**, 101907 (2012).

[126] S. Lany and A. Zunger, Phys. Rev. Lett. **100**, 016401 (2008).

[127] J. Pohl and K. Albe, Phys. Rev. B **87**, 245203 (2013).

[128] H. J. v. Bardeleben, Solar Cells **16**, 381 (1986).

[129] V. Depredurand, T. Bertram, and S. Siebentritt, Phys. B: Condens. Matter **439**, 101 (2014).

[130] A. Zunger, S. B. Zhang, and S.-H. Wei, in *26th IEEE PV Specialist Conference*, edited by P. Basore (American Institute of Physics, Melvin, NY, 1997), p. 313.

[131] S.-H. Wei, S. B. Zhang, and A. Zunger, Appl. Phys. Lett. **72**, 3199 (1998).

[132] S. B. Zhang, S.-H. Wei, A. Zunger, and H. Katayama-Yoshida, Phys. Rev. B **57**, 9642 (1998).

[133] J. Heyd, G. E. Scuseria, and M. Ernzerhof, J. Chem. Phys. **118**, 8207 (2003).

[134] A. Garza and G. E. Scuseria, J. Phys. Chem. Lett. **7**, 4165 (2016).

[135] L. E. Oikkonen, M. G. Ganchenkova, A. P. Seitsonen, and R. M. Nieminen, J. Phys.: Condens. Matter **26**, 345501 (2014).

[136] Y. S. Yee, B. Magyari-Köpe, Y. Nishi, S. F. Bent, and B. M. Clemens, Phys. Rev. B **92**, 195201 (2015).

[137] R. Saniz, J. Bekaert, B. Partoens, and D. Lamoen, Phys. Chem. Chem. Phys. **19**, 14770 (2017).

[138] J. Bekaert, R. Saniz, B. Partoens, and D. Lamoen, Phys. Chem. Chem. Phys. **16**, 22299 (2014).

[139] M. Han, Z. Zeng, T. Frauenheim, and P. Deák, Phys. Rev. B **96**, 165204 (2017).

[140] P. Deak, Q. D. Ho, F. Seemann, B. Aradi, M. Lorke, and T. Frauenheim, Phys. Rev. B **95**, 075208 (2017).

[141] J. Pohl, T. Unold, and K. Albe, arXiv:1205.2556.

[142] C. Lei, A. Rockett, I. M. Robertson, W. N. Shafarman, and M. Beck, J. Appl. Phys. **100**, 073518 (2006).

[143] C. M. Li, C. H. Lei, I. M. Robertson, and A. Rockett, Mater. Res. Soc. Symp. Proc. **763**, 169 (2003).

[144] D. Abou-Ras, S. S. Schmidt, N. Schäfer, J. Kavalakkatt, T. Rissom, T. Unold, R. Mainz, A. Weber, T. Kirchartz, E. Simsek Sanli, P. A. van Aken, Q. M. Ramasse, H.-J. Kleebe, D. Azulay, I. Balberg, O. Millo, O. Cojocaru-Mirédin, D. Barragan-Yani, K. Albe, J. Haarstrich, and C. Ronning, Phys. Status Solidi RRL **10**, 363 (2016).

[145] D. Barragan-Yani and K. Albe, Phys. Rev. B **95**, 115203 (2017).

[146] S. Lany and A. Zunger, J. Appl. Phys. **100**, 113725 (2006).

[147] S. A. Jensen, A. Kanevce, L. M. Mansfield, S. Glynn, S. Lany, and D. Kuciauskas, Sci. Rep. **7**, 13788 (2017).

[148] S. Lany and A. Zunger, Phys. Rev. B **72**, 035215 (2005).

[149] M. Ruckh, D. Schmid, M. Kaiser, R. Schäffler, T. Walter, and H. W. Schock, in *1st World Conference on Photovoltaic Energy Conversion* (IEEE, New York, 1994), p. 156.

[150] Z.-K. Yuan, S. Chen, Y. Xie, J.-S. Park, H. Xiang, X.-G. Gong, and S.-H. Wei, Adv. Energy Mater. **6**, 1601191 (2016).

[151] S.-H. Wei, S. B. Zhang, and A. Zunger, J. Appl. Phys. **85**, 7214 (1999).

[152] J. G. Simmons and G. W. Taylor, Phys. Rev. B **4**, 502 (1971).

[153] M. Turcu, O. Pakma, and U. Rau, Appl. Phys. Lett. **80**, 2598 (2002).

[154] H. Elanzeery, M. Melchiorre, M. Sood, F. Babbe, F. Werner, G. Brammertz, and S. Siebentritt, Phys. Rev. Mater. **3**, 055403 (2019).

[155] F. Babbe, L. Choubrac, and S. Siebentritt, Appl. Phys. Lett. **109**, 082105 (2016).

[156] D. Regesch, L. Gütay, J. K. Larsen, V. Depredurand, D. Tanaka, Y. Aida, and S. Siebentritt, Appl. Phys. Lett. **101**, 112108 (2012).

[157] L. Gütay, D. Regesch, J. K. Larsen, Y. Aida, V. Depredurand, A. Redinger, S. Caneva, S. Schorr, C. Stephan, S. Botti, J. Vidal, and S. Siebentritt, Phys. Rev. B **86**, 045216 (2012).

[158] K. Huang and A. Rhys, Proc. R. Soc. London, Ser. A **204**, 406 (1950).

[159] A. Krysztopa, M. Igalson, Y. Aida, J. Larsen, L. Gütay, and S. Siebentritt, J. Appl. Phys. **110**, 103711 (2011).

[160] A. Jasenek, U. Rau, V. Nadenau, and H. W. Schock, J. Appl. Phys. **87**, 594 (2000).

[161] G. Marín, C. Rincón, S. M. Wasim, G. Sánchez Pérez, and I. Molina, J. Alloys Compd. **283**, 1 (1999).

[162] L. Durán, C. Guerrero, E. Hernández, J. M. Delgado, J. Contreras, S. M. Wasim, and C. A. Durante Rincón, J. Phys. Chem. Solids **64**, 1907 (2003).

[163] M. Morkel, L. Weinhardt, B. Lohmüller, C. Heske, E. Umbach, W. Riedl, S. Zweigart, and F. Karg, Appl. Phys. Lett. **79**, 4482 (2001).

[164] J. Luckas, C. Longeaud, T. Bertram, and S. Siebentritt, Appl. Phys. Lett. **104**, 153905 (2014).